

Water Production Activity of Nine Long-Period Comets from SOHO/SWAN Observations of Hydrogen Lyman-alpha: 2013-2016

Short Title: Water Production in Comets 2013-2016

M.R. Combi¹, T.T. Mäkinen², J.-L. Bertaux³, E. Quémerais³,
S. Ferron⁴, M. Avery¹ and C. Wright¹

¹Dept. of Climate and Space Sciences and Engineering
University of Michigan
2455 Hayward Street
Ann Arbor, MI 48109-2143

*Corresponding author: mcombi@umich.edu

²Finnish Meteorological Institute, Box 503
SF-00101 Helsinki, FINLAND

³LATMOS/IPSL
Université de Versailles Saint-Quentin
11, Boulevard d'Alembert, 78280, Guyancourt, FRANCE

⁴ACRI-st, Sophia-Antipolis, FRANCE

36 Pages

3 Tables

10 Figures

9 Supplementary Tables

Submitted to Icarus

Abstract

Nine recently discovered long-period comets were observed by the Solar Wind Anisotropies (SWAN) Lyman-alpha all-sky camera on board the Solar and Heliosphere Observatory (SOHO) satellite during the period of 2013 to 2016. These were C/2012 K1 (PanSTARRS), C/2013 US10 (Catalina), C/2013 V5 (Oukaimeden), C/2013 R1 (Lovejoy), C/2014 E2 (Jacques), C/2014 Q2 (Lovejoy), C/2015 G2 (MASTER), C/2014 Q1 (PanSTARRS) and C/2013 X1 (PanSTARRS). Of these 9 comets 6 were long-period comets and 3 were possibly dynamically new. Water production rates were calculated from each of the 885 images using our standard time-resolved model that accounts for the whole water photodissociation chain, exothermic velocities and collisional escape of H atoms. For most of these comets there were enough observations over a broad enough range of heliocentric distances to calculate power-law fits to the variation of production rate with heliocentric distances for pre- and post-perihelion portions of the orbits. Comet C/2014 Q1 (PanSTARRS), with a perihelion distance of only ~ 0.3 AU, showed the most unusual variation of water production rate with heliocentric distance and the resulting active area variation, indicating that when the comet was within 0.7 AU its activity was dominated by the continuous release of icy grains and chunks, greatly increasing the active sublimation area by more than a factor of 10 beyond what it had at larger heliocentric distances. A possible interpretation suggests that a large fraction of the comet's mass was lost during the apparition.

Keywords: Comets, coma; Ices; Ultraviolet observations; Comets: C/2012 K1 (PanSTARRS), C/2013 US10 (Catalina), C/2013 V5 (Oukaimeden), C/2013 R1 (Lovejoy), C/2014 E2 (Jacques), C/2014 Q2 (Lovejoy), C/2015 G2 (MASTER), C/2014 Q1 (PanSTARRS), C/2013 X1 (PanSTARRS)

Introduction

The Solar Wind ANisotropies (SWAN) instrument on board the SOLar and Heliospheric Observatory (SOHO) satellite has been operating in a halo orbit around the Earth-Sun L1 Lagrange point since shortly after its launch on 2 December 1995. During that time it has recorded the hydrogen Lyman-alpha comae of over 70 comets, as well as multiple apparitions each of several short-period comets that have returned more than once since 1995; water production rates have been determined from these observations. Data from 63 comet apparitions observed from 1996 to 2012 have recently been archived in and certified by the NASA Planetary Data System Small Bodies node (Combi, 2017). A number of comets have been observed in the SWAN full-sky survey data since 2012, and here we present the results of water production rates calculated from nine long-period comets observed from 2013 through 2016. For most of the comets we derive pre- and post-perihelion power-law fits to the production rate variation with heliocentric distance. We also discuss each comet in the context of already published results.

Observations and Basic Model Analysis

While the SWAN instrument on the SOHO spacecraft was designed primarily to observe the interplanetary hydrogen distribution in the whole sky and monitor how it is affected by the changing solar wind, it was planned from the beginning that it would be an excellent instrument for observing comets (Bertaux et al., 1998). From its place in a halo orbit around the Sun-Earth L1 Lagrange point, most of the sky except for regions fairly close to the Sun and that obscured by the spacecraft itself, which also mostly blocks the Earth, is seen by SWAN. Unlike ground-based observatories, which have difficulty observing comets close to the local sunrise or sunset

horizon or those in the opposite hemisphere, SWAN can observe most comets that are bright enough, typically brighter than magnitude 10-12, most of the time, providing an excellent place to observe comets continuously over large portions of their orbits.

SWAN consists of a 5 x 5 array of 1-degree detectors that are scanned across the whole sky each day, creating a full sky map of hydrogen Lyman-alpha. Except for a special set of comet-specific observations of the Rosetta target comet 67P/Churyumov-Gerasimenko in 2009 (Bertaux et al., 2014), comets since 2007 have been observed only in the full sky images. This is also true for the comet results presented in this paper. Water production rates derived from a set of 65 apparitions of 50 comets (Combi, 2017) have recently been archived and certified in the Planetary Data System (PDS) Small Bodies Node (SBN) and can be found at URL https://pds-smallbodies.astro.umd.edu/holdings/pds4-soho:swan_derived-v1.0/SUPPORT/dataset.html. The results contained in the paper include comets observed after this first set, though these data will be archived in the PDS at some time.

The SWAN instrument and its use for observing comets has been discussed by Bertaux et al. (1998) and Combi et al. (2005), and the updated calibration of the instrument for comets was discussed by Combi et al. (2011a). Since atomic hydrogen in comets is produced mostly in the photodissociation chain of H₂O and OH it is possible to determine the water production rate in comets from observations of the hydrogen Lyman-alpha coma. The so-called time-resolved model used to calculate water production rates was presented and discussed in detail by Mäkinen and Combi (2005) and the determination of the various model parameters and parameterizations have been discussed in the Comets II review chapter by Combi et al. (2004). The fluorescence rate, or g-factor, of hydrogen atoms illuminated by the Sun is determined from the daily average solar irradiance compiled at LASP of the University of Colorado at the URL

<http://lasp.colorado.edu/lisird/lya/>. Because comets do not see the same face of the Sun as do the near-Earth satellites that contribute to the LASP solar measurements, we take the value from the nearest date corresponding to the heliographic longitude differences between the Earth and comet.

Nine long-period or dynamically new Oort cloud comets were observed during the period of 2013-2016 by SWAN. Orbital characteristics, time periods, and numbers of images are listed in Table 1. Table 1 contains the value of the original semi-major axis of the orbit (a_0) for each comet obtained from the Minor Planet Center (http://www.minorplanetcenter.net/db_search/). In the last column we have adopted the dynamical class scheme from the 85 comets photometric survey of A'Hearn et al. (1995) where dynamically new comets (DN) have semi-major axes larger than 20000 AU, Young Long-Period comets (YL) have semi-major axes between 500 and 2000 AU and Old Long-Period comets (OL) have semi-major axes less than 500 AU. It is estimated that ~90% of DN could be making their first trip into the inner solar system whereas most of the YL and OL comets have probably been to the planet region of the solar system before. The JPL Horizons web site was also used to estimate the original semi-major axis values. Most of the values were the same except for the DN comets of very large a_0 , but in all cases the classification assignments were the same.

Complete tables of water production rates are included with this paper as Supplementary information because of their length. Tables S1 through S9 provide observational parameters, water production rates and random stochastic 1-sigma uncertainties associated with noise in the data and the model fitting procedure that accounts for the subtraction of the H Ly α emission from the interplanetary background, which is typically on the order of 1 kilorayleigh. For most of the comets water production rates for both pre- and post-perihelion parts of the orbit have been

expressed as power laws as a function of heliocentric distance in the form $Q = Q(1\text{AU}) r^a$, where Q is the water production, $Q(1\text{AU})$ is the water production rate at a heliocentric distance of 1 AU, and r is the heliocentric distance of the comet in AU. Those results for all 9 comets are given in Table 2. In the following discussion section we will show the results for each comet and discuss the various implications and compare with other observations when available. When comparing water production rates determined from SWAN measurements of H Ly α emission we have estimated that there is a possible systematic uncertain of $\sim 30\%$ owing to a combination of instrument calibration, the model parameterization and the various model parameters.

Results of Model Analyses for Each Comet

C/2012 K1 (PanSTARRS). The H Ly α coma of comet C/2012 K1 (PanSTARRS) was observed by SWAN from 22 April to 6 December 2014 covering a range of heliocentric distances from 2.375 AU before perihelion to 1.912 AU after. It reached a perihelion distance of 1.0545 AU on 27.7 August 2014. Its original semi-major axis was 55000 AU. This, combined with its activity shallow production slope before perihelion and its normal behavior after perihelion, would indicate that it is likely a new Oort cloud comet on its first passage through the inner solar system. The results are given in Table S1. Figures 1 a & b show the water production rate as a function of time and heliocentric distance, respectively, over the apparition. The power-law variation of water production rate before and after perihelion shown as the solid lines in Figure 1b are given by $2.0 \times 10^{29} r^{-0.8}$ molecules s^{-1} and $1.9 \times 10^{29} r^{-2.4}$ molecules s^{-1} , respectively.

In some ways the variation of production rate is reminiscent of comet C/2009 P1 (Garradd), which was also dynamically new, with a flat but very irregular and unusual variation on the inbound pre-perihelion leg inside 2.1 AU and a more normal and rather steady $r^{-2.4}$ drop

after perihelion. Like Garradd (Combi et al., 2013; Bodewits et al., 2014), C/2012 K1 (PanSTARRS) is suspected of having an important icy grain halo before perihelion that likely dominates the water production rate. McKay et al. (2016) suggest that there is evidence in the radial distribution of gas emission from 2012 K1 from a range of observations with different aperture sizes, showing that there is an important extended source of gas. Their results, derived from relatively large-aperture Swift/UVOT observations of OH, are consistent with both the much larger aperture SWAN results shown here and the ground-based OH observations by Knight and Schleicher (2014), but they see a trend when comparing production rates from much smaller aperture observations.

C/2013 US10 (Catalina). SWAN observations of the Ly α coma of comet C/2013 US10 (Catalina) from 30 June 2015 to 18 February 2016 yielded water production rates of the comet corresponding to heliocentric distances of 2.12 AU before perihelion to 1.91 AU after. The comet reached its perihelion distance of 0.823 AU on 15 November 2015. Its original semi-major axis, like that of C/2012 K1 (PanSTARRS), was quite large at 14000 AU, which is just below the cut-off of the dynamically new class, and indicates that it may not have been on its first pass through the inner solar system. Its activity variation, as indicated by the power-law slopes, are only somewhat flatter than the canonical -2, as shown in Figure 2a and as a function of heliocentric distance in Figure 2b. The results are given in Table S2. The variation with heliocentric distance can be described with a power-law slope of -1.6 before perihelion and -1.9 after perihelion and an otherwise steady increase and decrease with no unusual irregular variations or outbursts. Water production rates are generally higher before perihelion than after.

C/2013 V5 (Oukaimeden). Comet C/2013 V5 (Oukaimeden) was discovered as part of the Morocco Oukaimeden Sky Survey (MOSS) carried out by the observatory in Oukaimeden, Morocco on 12 November 2013 (Guido et al., 2013). The comet reached a perihelion distance of 0.625 AU on 28 September 2014. SWAN obtained images of its H Ly α coma from 19 August 2014 at a heliocentric distance of 1.01 AU to 7 October 2014, only a week after perihelion as its production rate and brightness were dropping much more rapidly than the very flat rise before perihelion. It also appears to be a dynamically new comet from the Oort cloud. The water production rate is shown plotted as a function of time from perihelion in Figure 3. The results are given in Table S3. While there were not enough data after perihelion to describe the variation with a power-law fit, we were able to fit a power law to the pre-perihelion data $3.4 \times 10^{28} r^{-1.0}$ molecules s⁻¹. Comet C/2013 V5 (Oukaimeden), like C/2012 K1 (Pan STARRS), had an original semi-major axis of 55000 AU, putting it easily into the dynamically new group. The very flat slope is consistent with it being a dynamically new comet on its first passage into the inner solar system.

C/2013 R1 (Lovejoy). SWAN obtained useful images of the H Ly α coma of comet C/2013 R1 (Lovejoy) from 13 October 2013 to 14 March 2014. The comet reached its perihelion of 0.812 AU on 22 December 2013. It has an original semi-major axis of 365 AU, so it does not appear to be a dynamically new comet on its first pass from the Oort cloud. Figures 4a and 4b give the water production rates as a function of time from perihelion and heliocentric distance, r , that are also listed in Table S4. Power laws of the forms $7.6 \times 10^{28} r^{-2.2}$ molecules s⁻¹ and $9.1 \times 10^{28} r^{-1.6}$ molecules s⁻¹ can describe the variation with time.

Water production rates determined by Biver et al. (2014) from OH observations from the Institut de Radioastronomie Millimétrique (IRAM) at pre-perihelion heliocentric distances of 1.13, 0.92, and 0.83 are in excellent agreement with the SWAN derived values at the same times. Biver et al. also reported IRAM detections of complex organics ethylene glycol and formamide in comet 2013 R1 (Lovejoy) at the 0.02% level compared with water.

On the other hand, water production rates determined from water IR emissions with NIRSPEC at the Keck Observatory by Paganini et al. (2014) over the pre-perihelion heliocentric distance range from 1.35 to 1.16 AU are systematically a factor of 2 or more below the SWAN values and the one overlapping value from Biver et al. (2014). Similarly the ground-based near-ultraviolet OH production rates given by Opitom et al. (2015), after accounting for the ~ 0.82 OH yield from H₂O photodissociation (Combi et al., 2004), like the NIRSPEC/Keck observations given by Paganini et al. (2014), are systematically smaller by factors of 2 or more from the SWAN and IRAM rates.

Figure 4b also shows various water production rate measures for comet C/2013 R1 (Lovejoy) determined from different observations. Opitom et al. (2015) have adopted the OH Haser scale lengths and methods from A'Hearn et al. (1995) to calculate OH production rates. Schleicher and Osip (2002) has shown that in order to compare water production determined from OH observations with those of other methods that the production rates need to be corrected for the more appropriate vectorial model (Festou, 1981), which is more typically used by space-based ultraviolet observations of OH (e.g., Swift by Bodewits et al., 2014). A number of comparisons of water production rates determined from SWAN observations of atomic hydrogen have shown that the vectorial model approach normally corrects for this factor of ~ 2 (Combi et al., 2000, 2005). Therefore the factor of ~ 2 offset between the water production rates derived

from Opitom et al. and SWAN, determined here for the pre-perihelion period, is not surprising, but the factor of nearly 4 offset for the post-perihelion period is quite puzzling. It does appear that the variation with heliocentric distance between the two datasets is consistent during the periods of overlap.

In the case of 2009 P1 (Garradd) there was a correlation between observational aperture size and calculated water production rate that was consistent with the interpretation that much of the water production resulted from a spatially extended sublimation source of icy particles (Combi et al., 2013; Bodewits et al., 2014). However, 2009 P1 (Garradd) was a dynamically new comet while 2013 R1 (Lovejoy) was not. While the aperture size for the ground-based IR measurements (Paganini et al., 2017) are the smallest, the effect of aperture size from the ground-based OH observations are intermediate and not much different from the IRAM measurements (Biver et al., 2016), even though the IRAM water production rates are consistent with the SWAN determined results having by far the largest observational aperture. The explanation may have to await the publication of more results.

C/2014 E2 (Jacques). Like C/2013 R1 (PanSTARRS), C/2014 E2 (Jacques) appears to be a very long period comet, but is probably not on its first pass from the Oort cloud, given its original semi-major axis of only 365 AU. SWAN obtained useful detections of this comet over six months of its apparition from 3 April 2014 to 19 October 2014, and heliocentric distances from 1.8 AU before perihelion to 2.1 AU after. The variation with heliocentric distance was rather "normal" having an exponential slope of -2.4 before perihelion and -1.7 after, and a small asymmetry in activity with somewhat higher water production rates before than after perihelion, on the average. The largest measured production rate occurred about four weeks before

perihelion, however, there was a long period on either side of perihelion when the comet was not observable. Figures 5a and 5b show the variation of water production rate with time and with heliocentric distance, respectively. The numerical values are listed in Table S5. Figure 5b also shows the best fit power law with heliocentric distance, r in AU, expressed as $1.5 \times 10^{29} r^{-2.4}$ molecules s^{-1} and $1.1 \times 10^{29} r^{-1.7}$ molecules s^{-1} , respectively.

C/2014 Q2 (Lovejoy). Like 2013 R1 and 2014 E2 C/2014 E2 (Jacques), comet C/2014 Q2 (Lovejoy) is a very long period but not a new comet. Six months' worth of observations were obtained from SWAN full-sky images covering the period from 28 November 2014 to 28 June 2015 and including a perihelion distance of 1.29 AU on 30 January 2015. Heliocentric distances covered were from 1.58 AU before perihelion to 2.17 AU after.

The variation of water production over time is shown in Figure 6a. Despite the fact that most returning bright comets from the Oort cloud on long-period orbits observed by SWAN over the years tend to have rather typical variations with heliocentric distance and power-law slopes in the range from -1.5 to -2.5, the variation of water production of comet C/2014 Q2 (Lovejoy) is quite unusual. The peak production rate of 8×10^{29} molecules s^{-1} occurred about 20 days after perihelion and production rates were generally much larger after perihelion than before. The power-law fit to the pre-perihelion data shown in Figure 6b was also rather unusual, having rather two different components. From a heliocentric distance of 1.4 AU to perihelion the slope was a very steep -6.6, and in calculating the slope these data dominated the fit. However, for distances from 1.6 to 1.4 AU before perihelion the variation was more irregular and less steep with a slope closer to -3, which is more similar to the generally consistent post-perihelion slope of -3.4. The numerical results are listed in Table S6. The original semi-major axis of 500 AU, its

irregular activity behavior, both combined with its strong seasonal effect, imply that it is consistent with having a nucleus that is quite evolved after having had many passages into the inner solar system. Other than having a very long period and a large absolute production rate at 1 AU, its behavior is more like many Jupiter family comets.

In an important paper by Biver et al. (2015) showing the detection of 21 molecules, including ethyl alcohol and sugar, they find a water production rate of $(5.0 \pm 0.2) \times 10^{29}$ molecules s^{-1} from observations of OH made with the Nançay radio telescope during the few days around perihelion and $(7.5 \pm 0.3) \times 10^{29}$ molecules s^{-1} of H₂O made with the Odin satellite by Biver et al. (2016). From the combination they estimate the water production rate just before perihelion of 6.0×10^{29} molecules s^{-1} . These are consistent with the SWAN measurements during the same period.

Paganini et al. (2017) have reported observations of H₂O and HDO obtained with NIRSPEC at the Keck Observatory on 4 February 2015, just 1 day after the end of the period covered by Faggi et al. (2016), and report a water production rate of $(5.0 \pm 0.13) \times 10^{29}$ molecules s^{-1} , also in agreement with the values of SWAN to well within the expected uncertainty ranges.

Faggi et al. (2016) observed comet C/2014 Q2 (Lovejoy) on the 3 days following perihelion with the Giano spectrograph on the Telescopio Nazionale Galileo (TNG) telescope at LaPalma, Canary Islands, and found a water production rate of $(3.11 \pm 0.14) \times 10^{29}$ molecules s^{-1} . This appears systematically lower than the other measurement but is technically within the SWAN results when accounting for the possible $\pm 30\%$ systematic uncertainty from various model parameters and calibration. The results of Faggi et al. (2016) and Paganini et al. (2017) are indicated on Figure 6a.

Finally, unpublished results from the TRAPPIST observatory (Jehin, private communication) give a ground-based OH production rate on 7 January 2015 of $(2.71 \pm 0.30) \times 10^{29}$ molecules s^{-1} , which implies a water production rate of 3.30×10^{29} when dividing by the OH branching ratio of 0.82. This is compared with the SWAN value on the same day of 2.87×10^{29} molecules s^{-1} . These are within their respective uncertainty estimates.

C/2015 G2 (MASTER). SWAN obtained useful observations of comet C/2015 G2 (MASTER) from 7 April 2015 to 26 June 2015. The comet reached a perihelion distance of 0.78 AU on 23 May 2015. Given its orbit, it is likely to be a dynamically new comet from the Oort cloud. The water production rates plotted as a function of time in Figure 7 indicate a very irregular variation over its orbit. See Table S7 for the numerical results and observational aspects. A power law in heliocentric distance, r , can be fitted to the pre-perihelion variation, yielding an unremarkable production rate variation of $4.1 \times 10^{28} r^{-1.8}$ molecules s^{-1} . A conventional power law following perihelion does not seem to have any meaning as the production rate is simply irregular and very flat over that period.

There are not as yet any published water production rates for C/2015 G2 (MASTER). Jehin (private communication) has reported an OH production rate on 21 April 2015, which when converted as above to a water production rate yields a value of 3.26×10^{28} molecules s^{-1} that compares favorably to the SWAN value on the same day of 3.86×10^{28} molecules s^{-1} . The original semi-major axis of this comet is 30400 AU, which puts it into the dynamically new category. While its inbound slope is not much flatter than -2, its very irregular variation both pre- and post-perihelion could be consistent with a first-time passage into the inner solar system.

C/2014 Q1 (PanSTARRS). The apparition of comet C/2014 Q1 (PanSTARRS) was quite short, covering only 90 days from 20 May 2015 through 10 August 2015. During that time the water production rate rose very rapidly to a value of almost 2×10^{30} molecules s^{-1} a few days before its relatively short perihelion distance of 0.32 AU from the Sun on 6 July 2015. It also declined similarly and very rapidly after perihelion. The water production rate, as determined from the SWAN observations of the H Ly α coma, is plotted as a function of time from perihelion in Figure 8. The numerical values are given in Table S8. It appears to be a very long period comet but not dynamically new on its first trip to the inner solar system from the Oort cloud, having an original semi-major axis of 825 AU. Its production rate can be well described by two power laws of the form $5.3 \times 10^{26} r^{-7.8}$ molecules s^{-1} pre-perihelion and $9.1 \times 10^{26} r^{-8.9}$ molecules s^{-1} post-perihelion.

The very steep rise near the very small heliocentric distances is reminiscent of comet C/2012 S1 (ISON), which began an extremely rapid increase in activity about 15 days before perihelion at a heliocentric distance of 0.70 AU, at which time its active area increased markedly compared with the more normal constant active area before that time (Combi et al., 2014). The interpretation for comet C/2012 S1 (ISON) is that its small nucleus began to disrupt, shedding icy grains and chunks at an increasing rate until its demise at its extremely small perihelion distance of less than 2 solar radii. If one only considers the variation of water production for heliocentric distances larger than ~ 0.7 AU, that is more than about 25 days on either side of perihelion, like ISON, the variation of C/2014 Q1 (PanSTARRS) is somewhat irregular, but rather flat.

Not all comets with very small perihelion distances exhibit this kind of behavior. A study of four comets with small perihelia, namely C/2002 V1 (NEAT), C/2002 X5 (Kudo–Fujikawa),

2006 P1 (McNaught) and 96P/Machholz 1, of 0.099, 0.190, 0.170 and 0.13 AU, respectively, all had reasonably normal variations with heliocentric distance with power-law slopes in the range of -1.5 to -3.5, pre- and post-perihelion (Combi et al., 2011b). So simply having a comet move very close to the Sun does not initiate this intense level of activity that greatly exceeds that which might be expected from some combination of a moderate seasonal effect in combination with water-dominated sublimation. This would imply that there was something different in the structure of comets C/2012 S1 (ISON) and C/2014 Q1 (PanSTARRS) than many other comets that pass well within 0.7 AU from the Sun but continue to sublimate steadily.

Circumstantial evidence might suggest that C/2014 Q1 (PanSTARRS) is probably similar to C/2012 S1 (ISON), and that it similarly began to rapidly shed chunks of nucleus material once it was closer to the Sun than about 0.7 AU, at which time the water production began to increase far more rapidly than something close to a constant cross-sectional area exposed to sunlight can. The fact that the post-perihelion activity level returned to a similar but slightly lower level once the comet returned to 0.7 to 1.0 AU suggests, however, that, unlike C/2012 S1 (ISON), a reasonable fraction of the nucleus remained intact after the apparition. This was also aided by the fact that the perihelion distance was not nearly as close as C/2012 S1 (ISON).

Figure 9 shows a plot of the active area of comet C/2014 Q1 (PanSTARRS) calculated following the method of Cowan and A'Hearn (1979), as done for comet C/2012 S1 (ISON) by Combi et al. (2014). It shows two relatively steady regions before 20 days before perihelion and after 20 days after perihelion, with up to 100 km² during the period around perihelion. The average active area of the steady region well before perihelion, shown as the thick solid line on the left part of the plot, has a value of 9.6 km², which is about 1.5 times larger than the value of 6 km² found for comet C/2012 S1 (ISON) well before perihelion. On the right side of the plot the

average active area, once it returns to another relatively steady level, is 4.9 km². From this we can conclude that the comet lost about half of its material during the very active phase near perihelion when it was shedding material with a total surface area of up to six times the original surface area of the nucleus.

The total water mass released during the whole observed apparition of ± 40 days from perihelion is 3.1×10^{11} kg, with about 90% of this released from the enhanced active area peak of ± 25 days from perihelion and about 10% from what would be the nucleus itself as determined by the flatter steady release before and after 25 days from perihelion. For comparison, this is a hundred times more than comet 67P/Churyumov-Gerasimenko, which lost about 3×10^9 kg during each orbit in 1996, 2002 and 2007 (Bertaux, 2015). This is also far larger than the mass comet C/2012 S1 (ISON) lost with the complete disruption of its nucleus (Combi et al., 2014). If the material in the nucleus of C/2014 Q1 (PanSTARRS) is assumed to be homogeneous, the reduction of active area would imply a decrease of the nucleus radius to 71% of its original size and a loss of 64% of its original total mass. The actual size of the nucleus will depend on the ratio of the water mass to the total mass. If we assume the same bulk nucleus density as 67P/Churyumov-Gerasimenko from Rosetta measurements (Pätzold et al., 2016) of 533 kg/m³, we can estimate the radius of the nucleus before and after perihelion for a few values of the water-to-total mass ratio.

These are given in Table 3 for values of the water to total mass ratio of 1, 1/2, 1/3 and 1/4. This ratio roughly corresponds to the inverse of the dust-to-gas mass ratio. For this fairly wide range of values, we find nucleus radii before the peak of the apparition in the range of 725 to 1151 meters. This indicates the nucleus of C/2014 Q1 (PanSTARRS) was quite a bit larger than

that of C2012 S1 (ISON), which completely disintegrated on its extremely close pass by the Sun, however it did lose most of its mass on this passage.

C/2013 X1 (PanSTARRS). Comet C/2013 X1 (PanSTARRS) is a young long-period (YL) comet, having an original semi-major axis of 4450 AU, and is not likely on its first trip into the inner solar system from the Oort cloud. Its H Ly α coma was detected in 121 full-sky SWAN images from 1 January 2016 to 21 June 2016. It reached a perihelion distance of 1.31 AU on 20 April 2016. It reached a peak water production rate of 4.4×10^{29} molecules s⁻¹ 15 days before perihelion. Water production rates and observational geometry parameters are given in Table S9.

Water production rates are plotted in Figure 10a as a function of time from perihelion in days and with pre- and post-perihelion data plotted as a function of heliocentric distance in Figure 10b. Table S9 gives the numerical values, uncertainties and observational parameters. This comet has a general variation over its orbit that can be expressed as a power law in heliocentric distance, r in AU, as $8.2 \times 10^{29} r^{-3.0}$ molecules s⁻¹ before perihelion and $2.7 \times 10^{29} r^{-2.2}$ molecules s⁻¹ after. Throughout March 2014 just before perihelion the comet could not be observed as it was in the solar avoidance area of the sky. Just after it was detectable again, the production rate started what appears to be an outburst that peaked two days later. The outburst lasted about 12 days and returned to the pre-perihelion value of just over 10^{29} molecules s⁻¹ a few days before perihelion. SWAN has a fairly small solar avoidance angle so it is doubtful that there are any (or many) observations of the comet during the period just before the outburst. After perihelion the comet's production rate generally drops fairly steadily as heliocentric distance increases.

Summary

We presented the results of a model analysis of over 800 images of the hydrogen Lyman-alpha comae of 6 long-period and 3 dynamically new comets observed with the SWAN all-sky camera on the SOHO spacecraft during the period of 2012 to 2016. Water production rates were calculated from each of the images with our standard method (Mäkinen and Combi, 2005). Regarding water production rates and activity over the orbits of the comets observed, two of the three comets, C/2012 K1 (PanSTARRS) and C/2013 V5 (Oukaimeden), fell into the dynamically new class and displayed the rather flat variations on their inbound orbits that one might expect for comets on their first trips into the inner solar system. The overall slope of -1.8 of the inbound variation of the third, C/2015 G2 (MASTER), was not particularly flat, but the variation was highly irregular both pre- and post-perihelion, and the post-perihelion was so irregular that fitting a power law was not meaningful. The remaining six long-period comets showed a wide range of variations with two having very steep variations, -6.6 and -3.4 slopes for C/2014 Q2 (Lovejoy) and -7.8 and -8.9 for C/2014 Q1 (PanSTARRS) pre- and post-perihelion, respectively.

Where available we compared the SWAN water production rates with some obtained either by water directly in the IR or inferred from OH ground-based observations. For some comets and some datasets agreement is quite good, while for others there are sometimes apparent systematic differences that have been seen in previous comparisons of other comets.

The most remarkable was comet C/2014 Q1 (PanSTARRS), which at first look presented very steep average power-law slopes of -7.8 and -8.9 before and after perihelion, respectively. A closer examination of the variation of water production rate over time showed that the rapid rise was confined to a period of within ± 25 days of perihelion while the comet was roughly within 0.7 AU from the Sun. Outside that period the activity was somewhat irregular but generally

steady. Calculations of the active area using the standard method of Cowan and A'Hearn (1979) showed that the equivalent active area was nearly a factor of ten larger during the perihelion time ($r_H \sim 0.31\text{AU}$) than both well before and after perihelion, and that the average active area well after perihelion was only half of the value well before perihelion. This behavior was generally similar to that of comet C/2012 S1 (ISON) covering the same heliocentric distances. However, both comets showed activity consistent with the shedding of large amounts of icy grains and chunks from their nuclei when they were within 0.7 AU from the Sun greatly increasing their active sublimation areas. While comet C/2012 S1 (ISON) did not survive intact its extremely small (< 2 solar radius) perihelion passage, comet C/2014 Q1 (PanSTARRS) did survive its more moderate 0.31 AU perihelion but had an active area about a factor of two smaller after perihelion than before, indicating that perhaps 64% of its original mass was lost, and its radius was reduced to 71% of its incoming value. Lastly, there are, of course, many comets that reach perihelion distances much smaller than 0.3 AU but exhibit normal activity (Combi et al., 2011a) and no evidence of greatly increased active surface area resulting from a violent release of icy grains and chunks from the nucleus.

Acknowledgements

We thank the two referees, Dr. Michael DiSanti and Dr. David Schleicher, for their careful reading and helpful comments, which have greatly improved this paper. SOHO is a cooperative international mission of ESA and NASA. M. Combi acknowledges support from grant NNX15AJ81G from the Solar System Observations Planetary Astronomy Program and NNX13AQ66G from the Planetary Mission Data Analysis Program. T.T. Mäkinen was supported by the Finnish Meteorological Institute (FMI). J.-L. Bertaux and E. Quémerais

acknowledge support from CNRS and CNES. We obtained cometary ephemerides and orbital elements from the JPL Horizons web site (<http://ssd.jpl.nasa.gov/horizons.cgi>). We obtained original semi-major axis values for each of the observed comets from the IAU Minor Planet Center (http://www.minorplanetcenter.net/db_search/). The composite solar Lyman-alpha data were obtained from the LASP web site at the University of Colorado (<http://lasp.colorado.edu/lisird/lya/>). We also gratefully acknowledge the personnel that have been keeping SOHO and SWAN operational for over 20 years, in particular Dr. Walter Schmidt at FMI.

References

- A'Hearn, M.F., Millis, R.C., Schleicher, D.G., Osip, D.J., Birch, P.V., 1995. The ensemble properties of comets: Results from narrowband photometry of 85 comets, 1976-1992. *Icarus* 118, 223–270, doi:10.1006/icar.1995.1190.
- Bertaux, J.L., 2014. Estimate of the erosion rate from H₂O mass-loss measurements from SWAN/SOHO in previous perihelions of comet 67P/Churyumov-Gerasimenko and connection with observed rotation rate variations. *Astron. Astrophys.* 583, A38, doi: 10.1051/0004-6361/201525992.
- Bertaux, J.L., et al., 1998. Lyman-alpha observations of comet Hyakutake with SWAN on SOHO. *Planet. Sp. Sci.* 46, 555–568, doi:10.1016/S0032-0633(97)00179-7.
- Biver, N., et al., 2014. Complex organic molecules in comets C/2012 F6 (Lemmon) and C/2013 R1 (Lovejoy): Detection of ethylene glycol and formamide. *Astron. Astrophys.* 566, L5, doi:10.1051/0004-6361/201423890.

- Biver, N., et al., 2015. Ethyl alcohol and sugar in comet C/2014 Q2 (Lovejoy). *Sci. Adv.* 1, e1500863, doi:10.1126/sciadv.1500863.
- Biver, N., et al., 2016. Isotopic ratios of H, C, N, O, and S in comets C/2012 F6 (Lemmon) and C/2014 Q2 (Lovejoy). *Astron. Astrophys.* 589, A78, doi: 10.1051/0004-6361/201528041.
- Bodewits, D., et al., 2014. The evolving activity of the dynamically young comet C/2009 P1 (Garradd). *Astrophys. J.* 768:48, doi:10.1088/0004-637X/786/1/48.
- Combi, M., 2017. SOHO SWAN Derived Cometary Water Production Rates Collection, urn:nasa:pds:soho:swan_derived::1.0, L. Feaga (ed), NASA Planetary Data System.
- Combi, M.R., Reinard, A.A., Bertaux, J.-L., Quémérais, E., Mäkinen, T., 2000. SOHO/SWAN observations of the structure and evolution of the hydrogen Lyman- α coma of Comet Hale-Bopp (1995 O1). *Icarus* 144, 191–202, doi:10.1006/icar.1999.6335.
- Combi, M.R., Harris, W.M., Smyth, W.H., 2004. Gas dynamics and kinetics in the cometary coma: Theory and observations. In: Festou, M.C., Keller, H.U., and Weaver, H.A. (Eds.), *Comets II*, Univ. Arizona Press, pp. 523–552.
- Combi, M.R., Mäkinen, J.T.T., Bertaux, J.-L., Quémérais, E., 2005. Temporal deconvolution of the hydrogen coma. II. Pre- and post-perihelion activity of Comet Hyakutake (1996 B2). *Icarus* 177, 228–245, doi: 10.1016/j.icarus.2005.03.007.
- Combi, M.R., Lee, Y., Patel, T.S., Mäkinen, J.T.T., Bertaux, J.-L., Quémérais, E., 2011a. SOHO/SWAN observations of short-period spacecraft target comets. *Astron. J.* 141:128, doi: 10.1088/0004-6256/141/4/128.
- Combi, M.R., et al., 2011b. SOHO/SWAN observations of comets with small perihelia: C/2002 V1 (NEAT), C/2002 X5 (Kudo-Fujikawa), 2006 P1 (McNaught) and 96P/Machholz 1. *Icarus* 216, 449–461, doi:10.1016/j.icarus.2011.09.019.

- Combi, M.R., Mäkinen, J.T.T., Bertaux, J.-L., Quémerais, E., Ferron, S., Fougere, N., 2013. Water production rate of Comet C/2009 P1 (Garradd) throughout the 2011-2013 apparition: Evidence for an icy grain halo. *Icarus* 225, 740–748, doi: 10.1016/j.icarus.2013.04.030.
- Combi, M.R., Fougere, N., Mäkinen, J.T.T., Bertaux, J.-L., Quémerais, E., Ferron, S., 2014. Unusual water production activity of Comet C/2012 S1 (ISON): Outbursts and continuous fragmentation. *Astrophys. J. Lett.* 788:L7, doi:10.1088/2041-8205/788/1/L7.
- Cowan, J.J., A'Hearn, M.F., 1979. Vaporization of comet nuclei - Light curves and life times. *Moon & Planets* 21, 155–171, doi:10.1007/BF00897085.
- Faggi, S., et al., 2016. Detailed analysis of near-IR water (H₂O) emission in comet C/2017 Q2 (Lovejoy) with the Giano/TNH spectrograph. *Astrophys. J.* 830:157, doi: 10.3847/0004-637X/830/2/157.
- Festou, M.C., 1981. The density distribution of neutral compounds in cometary atmospheres. I - Models and equations. *Astron. Astrophys.* 95, 69–79.
- Guido, E., et al., 2013. Comet C/2013 V5 (Oukaimeden). CBET 3713.
- Knight, M.M., Schleicher, D.G., 2014. Coma morphology of recent comets: C/ISON (2012 S1), C/Pan-STARRS (2012 K1), C/Jacques (2014 E2), and C/Siding Spring (2013 A1). In: *Am. Astron. Soc. – Div. Planet. Sci. Meet. #46*, abstract 209.20.
- Mäkinen, J.T.T., Combi, M.R., 2005. Temporal deconvolution of the hydrogen coma I. A hybrid model. *Icarus* 177, 217–227, doi:10.1016/j.icarus.2005.02.010.
- McKay, A.J., et al., 2016. The CO₂ abundance in comets C/2012 K1 (PanSTARRS), C/2012 K5 (LINEAR), and 290P/Jäger as measured with Spitzer. *Icarus* 266, 249–260, doi: 10.1016/j.icarus.2015.11.004.

- Opitom, C., Jehin, E., Manfroid, J., Hutsemékers, D., Gillon, M., Magain, P., 2015. TRAPPIST photometry and imaging monitoring of comet C/2013 R1 (Lovejoy): Implications for the origin of daughter species. *Astron. Astrophys.* 584, A121, doi:10.1051/0004-6361/201526427.
- Paganini, L., et al., 2014. C/2013 R1 (Lovejoy) at IR wavelengths and the variability of CO abundances among Oort Cloud comets. *Astrophys. J.* 791:122, doi:10.1088/0004-637X/791/2/122.
- Paganini, L., Mumma, M.J., Gibb, E.L., Villanueva, G.L., 2017. Ground-based detection of deuterated water in comet C/2014 Q2 (Lovejoy) at IR wavelengths. *Astrophys. J. Lett.* 836:L25, doi: 10.3847/2041-8213/aa5cb3.
- Pätzold, M., et al., 2016. A homogeneous nucleus for comet 67P/Churyumov-Gerasimenko from its gravity field. *Nature* 530, 63–65, doi: 10.1038/nature16535.
- Roth, N.X., et al., 2017. The composition of comet C/2012 K1 (PanSTARRS) and the distribution of primary volatile abundances among comets. *Astron. J.* 153:168, doi: 10.3847/1538-3881/aa5d18.
- Schleicher, D.G., Osip, D.J., 2002. Long- and short-term photometric behavior of comet Hyakutake (1996 B2). *Icarus* 159, 210–233, doi: 10.1006/icar.2002.6875.

Table 1. Comets Observed with SWAN, Data Description and Orbital Parameters

Comet	q(AU)	a_0 (AU) ^a	r_H (AU) ^b	No. of images	Class ^c
C/2012 K1 (PanSTARRS)	1.0545 27.7 Aug 2014	55340	2.197 - 1.055 1.055 - 1.912	138	DN
C/2013 US10 (Catallina)	0.8230 15.7 Nov 2015	14430	2.375 - 0.950 0.869 - 1.823	119	YL
C/2013 V5 (Oukaimeden)	0.6255 28.2 Sep 2014	55160	1.010 - 0.626 0.633 - 0.666	41	DN
C/2013 R1 (Lovejoy)	0.8115 22.7 Dec 2013	365	1.468 - 0.812 0.812 - 1.701	141	OL
C/2014 E2 (Jacques)	0.6639 2.5 Jul 2013	790	1.763 - 0.837 0.699 - 2.066	97	YL
C/2014 Q2 (Lovejoy)	1.290 30.1 Jan 2015	500	1.583 - 1.291 1.291 - 2.172	138	OL/YL
C/2015 G2 (MASTER)	0.7798 23.8 May 2015	30400	1.159 - 0.781 0.780 - 1.014	59	DN
C/2014 Q1 (PanSTARRS)	0.3146 6.5 Jul 2015	826	1.189 - 0.335 0.495 - 0.958	31	YL
C/2013 X1 (PanSTARRS)	1.3143 20.8 Apr 2016	4500	2.235 - 1.314 1.314 - 1.972	121	YL

a. The original semi-major axis before the perihelion passage.

b. For each comet the heliocentric distance range is given for pre- and post-perihelion periods.

c. Dynamical classes are DN (Dynamically New), OL (Old Long Period), YL (Young Long Period) as discussed in the text.

Table 2. Water Production Rate Heliocentric Distance Dependencies

Comet	Q Pre-Perihelion ^a	Q Post-Perihelion ^a
C/2012 K1 (PanSTARRS)	$2.0 \times 10^{29} r^{-0.8}$	$1.9 \times 10^{29} r^{-2.4}$ ¹
C/2013 US10 (Catalina)	$2.8 \times 10^{29} r^{-1.6}$	$1.6 \times 10^{29} r^{-1.9}$
C/2013 V5 (Oukaimeden)	$3.4 \times 10^{28} r^{-1.0}$	-
C/2013 R1 (Lovejoy)	$7.6 \times 10^{28} r^{-2.2}$	$9.1 \times 10^{28} r^{-1.6}$
C/2014 E2 (Jacques)	$1.5 \times 10^{29} r^{-2.4}$	$1.1 \times 10^{29} r^{-1.7}$
C/2014 Q2 (Lovejoy)	$2.3 \times 10^{30} r^{-6.6}$	$1.9 \times 10^{30} r^{-3.4}$
C/2015 G2 (MASTER)	$4.1 \times 10^{28} r^{-1.8}$	-
C/2014 Q1 (PanSTARRS)	$5.3 \times 10^{26} r^{-7.8}$	$9.1 \times 10^{26} r^{-8.9}$
C/2013 X1 (PanSTARRS)	$8.2 \times 10^{29} r^{-3.0}$	$2.7 \times 10^{29} r^{-2.2}$

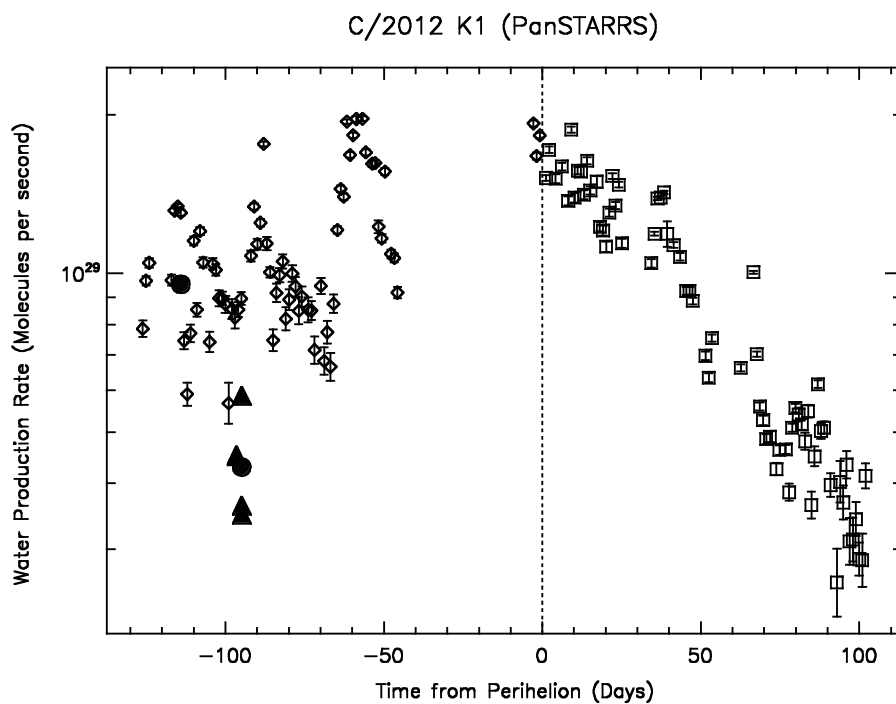
a. Production rate at 1 AU in molecules s⁻¹.

Table 3. Estimates of a Spherical Nucleus Radius Loss for C/2014 Q1 (PanSTARRS)

Water mass fraction of the nucleus	f=1	f=1/2	f=1/3	f=1/4
Total mass loss ± 40 days (kg)	3.1×10^{11}	6.2×10^{11}	9.3×10^{11}	12.4×10^{11}
Radius before -25 days (m)	725	913	1045	1151
Radius after +25 days (m)	515	648	741	816

f = the water mass fraction of the nucleus

(a)



(b)

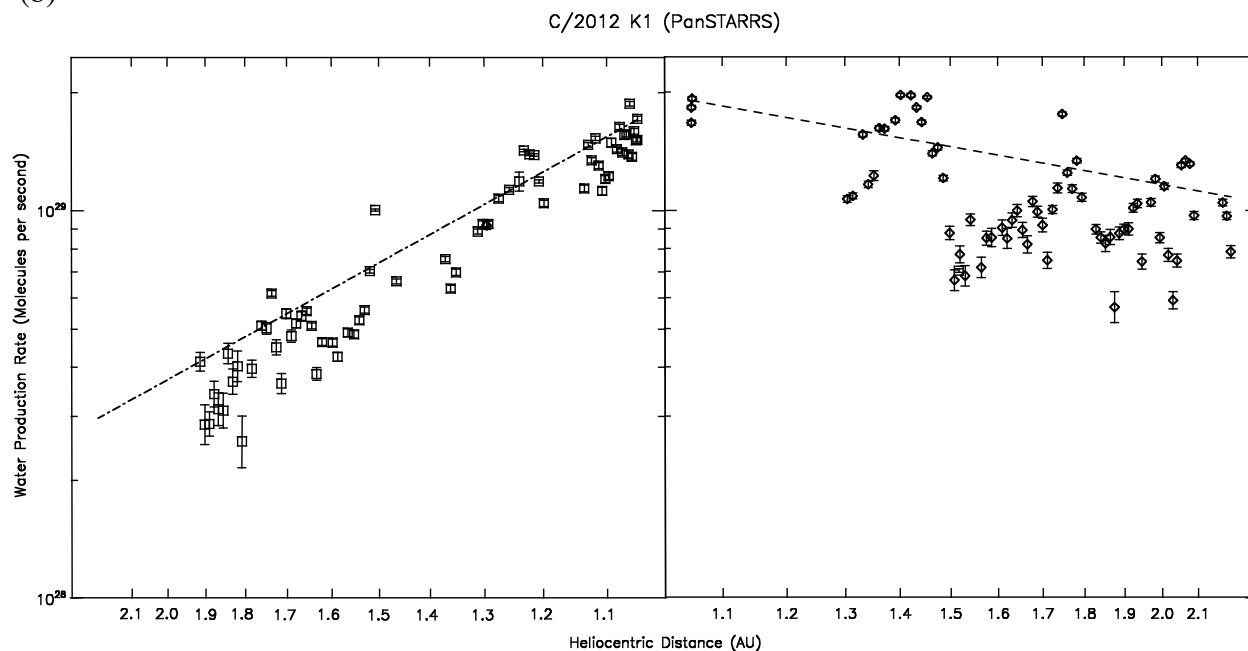
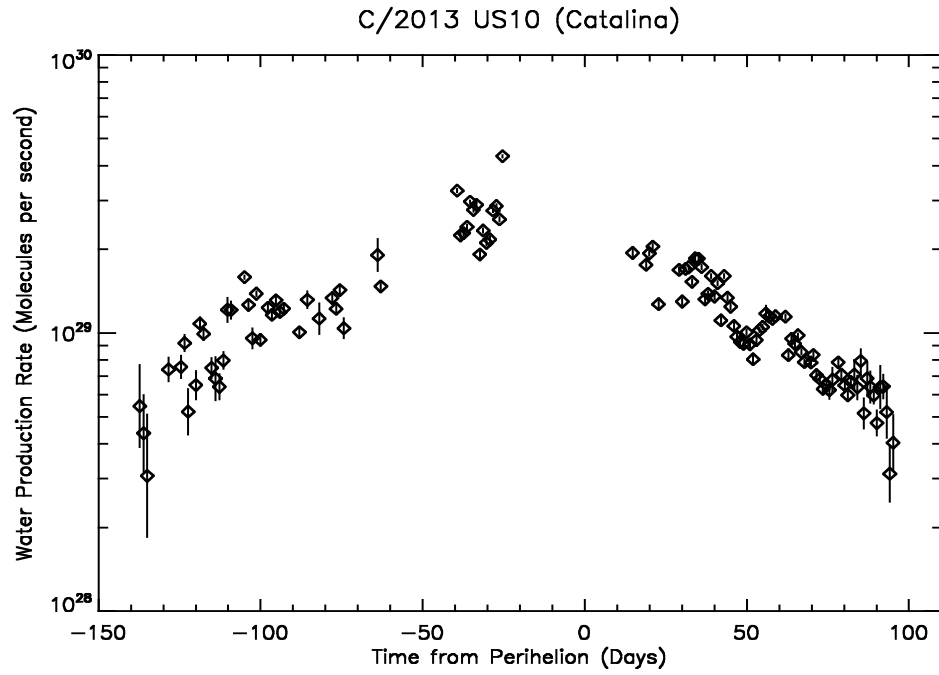


Fig. 1. Water production rate in comet C/2012 K1 (PanSTARRS) (a) shows the variation over time in days from perihelion, and (b) shows the variation with heliocentric distance with the diamonds giving the pre-perihelion values and the squares giving the post-perihelion values. The error bars correspond to the 1-sigma stochastic errors from noise in the data and the model fitting. The lines give the best-fit power-law variation with form given in Table 2. Shown in (a) are the measurements of McKay et al. (2016) as filled circles and of Roth et al. (2017) as filled triangles.

(a)



(b)

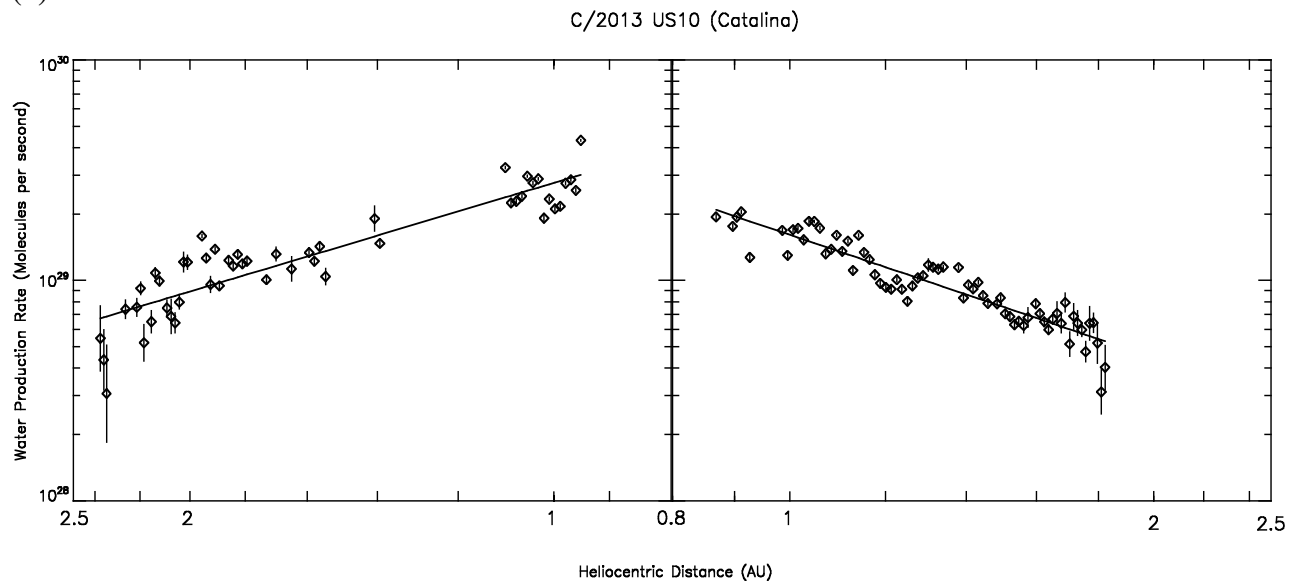


Fig. 2. Water production rate in comet C/2013 US10 (Catalina). (a) Variation over time in days from perihelion. (b) Variation with heliocentric distance. The error bars correspond to the 1-sigma stochastic errors from noise in the data and the model fitting. The lines give the best-fit power-law variation with form given in Table 2.

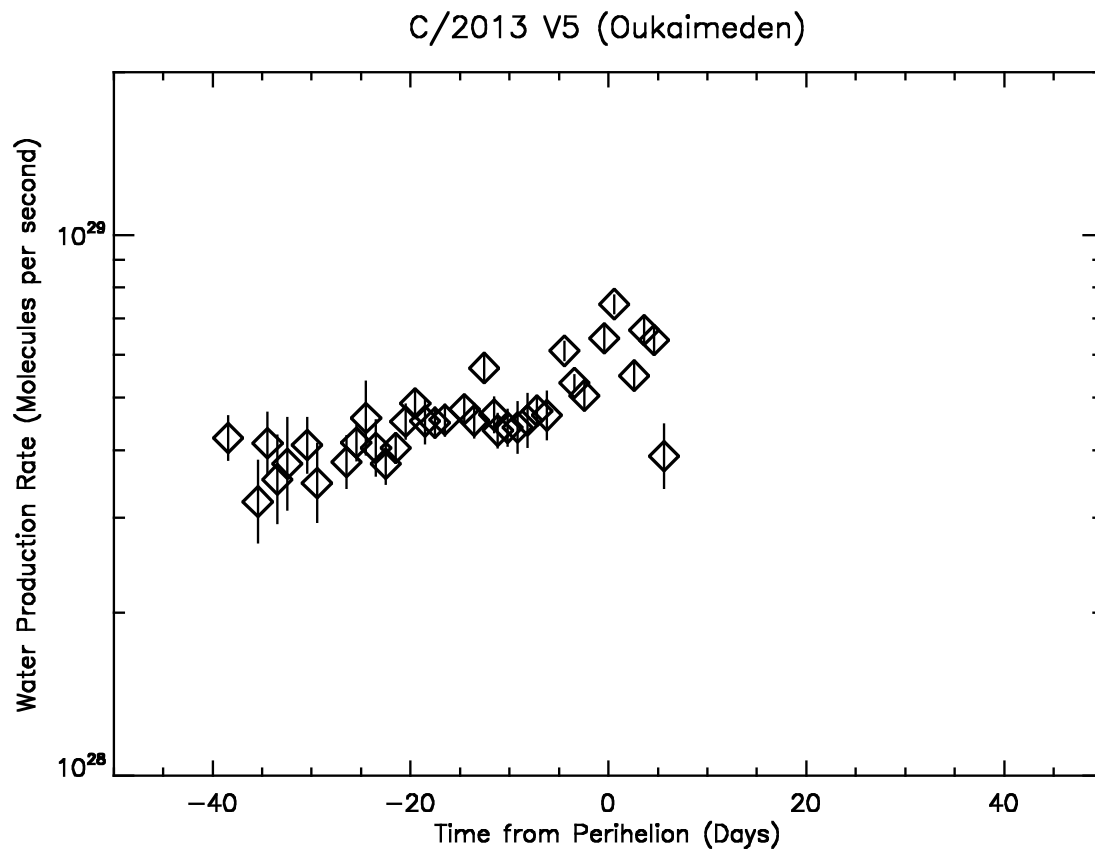


Fig. 3. Water production rate in comet C/2013 V5 (Oukaimeden) over time in days from perihelion. The error bars correspond to the 1-sigma stochastic errors from noise in the data and the model fitting.

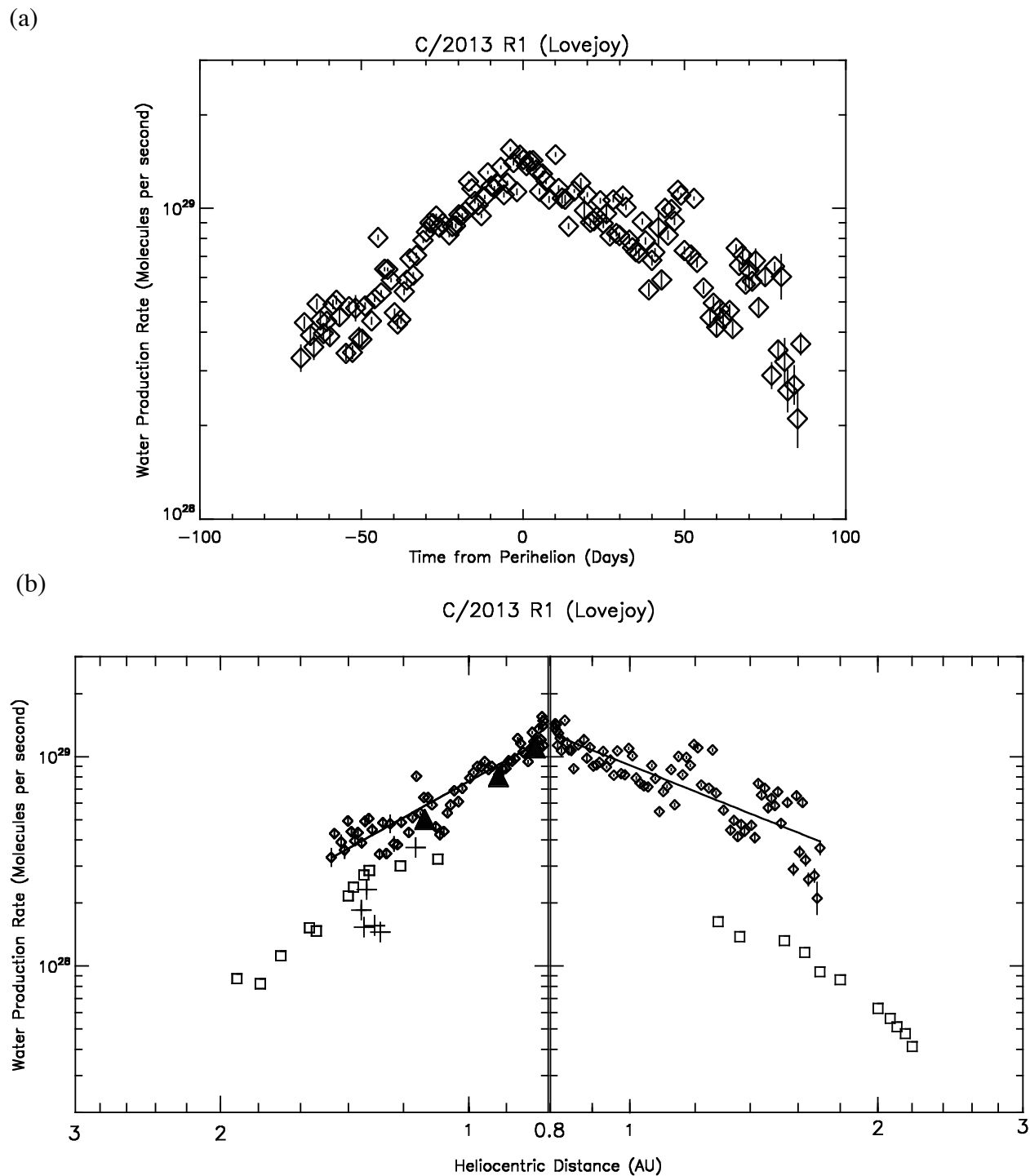


Fig. 4. Water production rate in comet C/2013 R1 (Lovejoy). (a) Variation over time in days from perihelion. (b) Variation with heliocentric distance. The error bars correspond to the 1-sigma stochastic errors from noise in the data and the model fitting. The lines give the best-fit power-law variation with form given in Table 2. The pluses give the production rates from Paganini et al. (2014), the filled triangles from Biver et al. (2014) and the squares from Opitom et al. (2015). The diamonds give the values from the SWAN measurements.

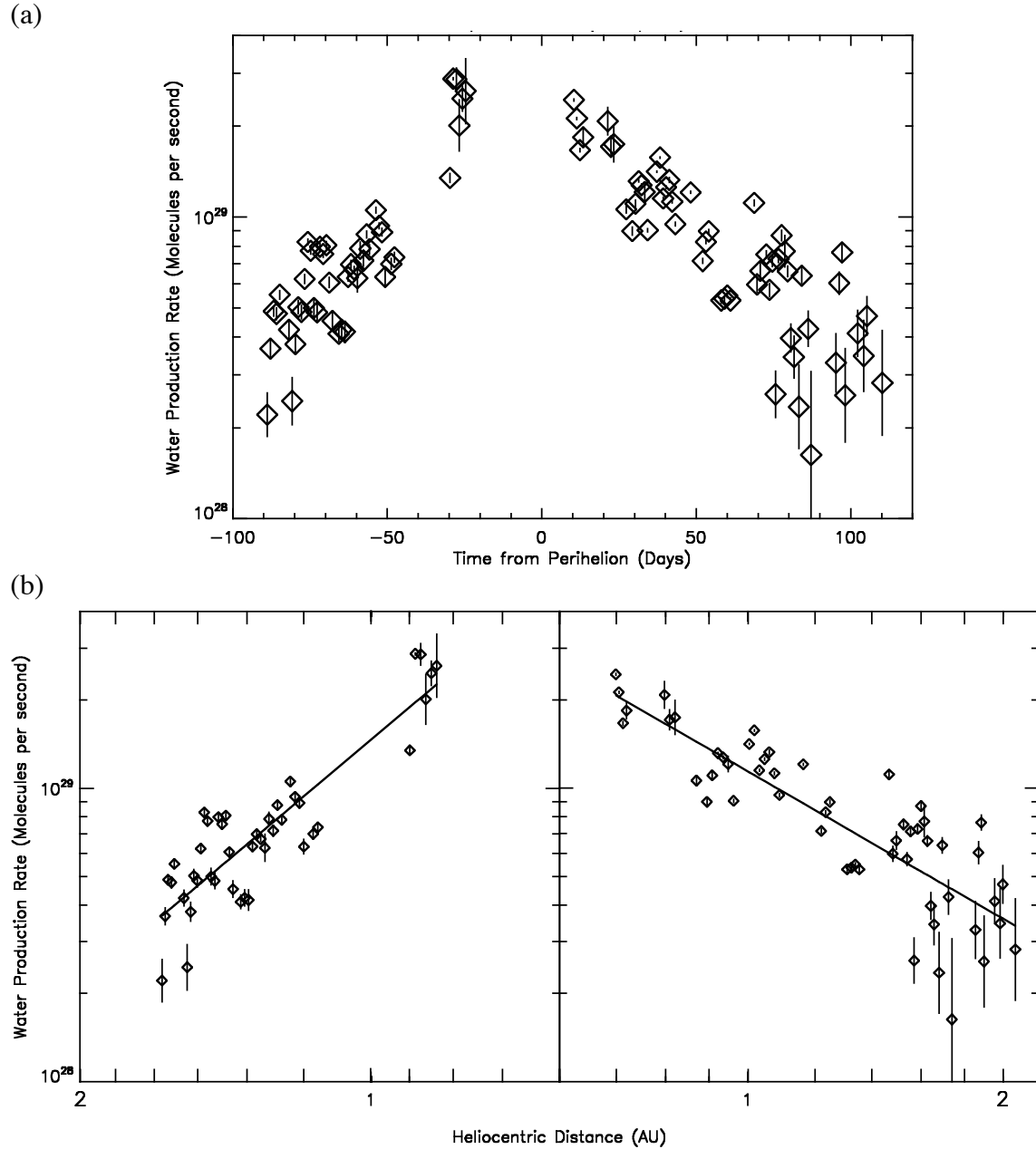


Fig. 5. Water production rate in comet C/2014 E2 (Jacques). (a) Variation over time in days from perihelion. (b) Variation with heliocentric distance. The error bars correspond to the 1-sigma stochastic errors from noise in the data and the model fitting. The lines give the best-fit power-law variation with form given in Table 2.

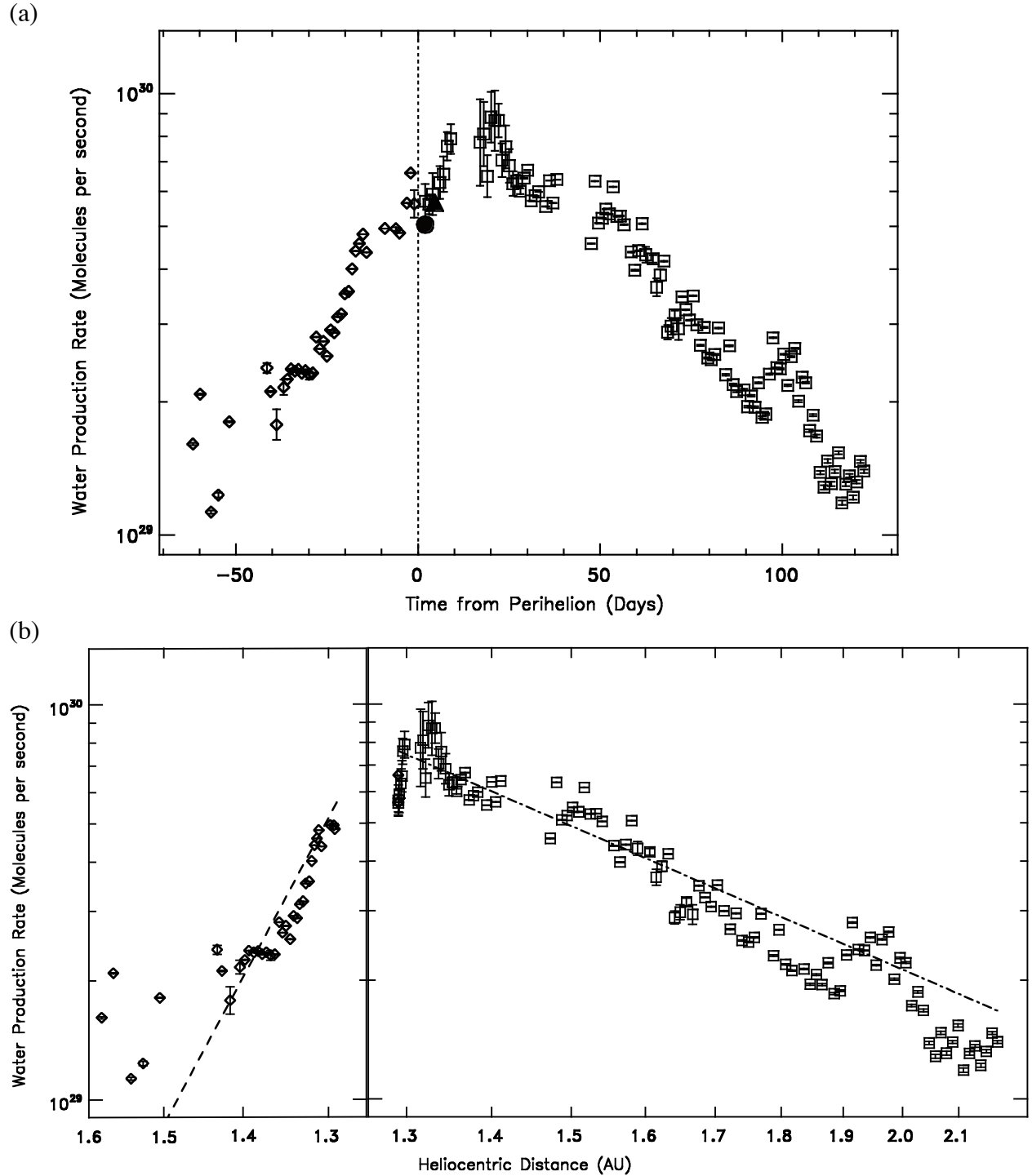


Fig. 6. Water production rate in comet C/2014 Q2 (Lovejoy). (a) Variation over time in days from perihelion. (b) Variation with heliocentric distance. The error bars correspond to the 1-sigma stochastic errors from noise in the data and the model fitting. The lines give the best-fit power-law variation with form given in Table 2. The filled circle in (a) shows the result from Faggi et al. (2016) and the filled triangle shows the result from Paganini et al. (2017).

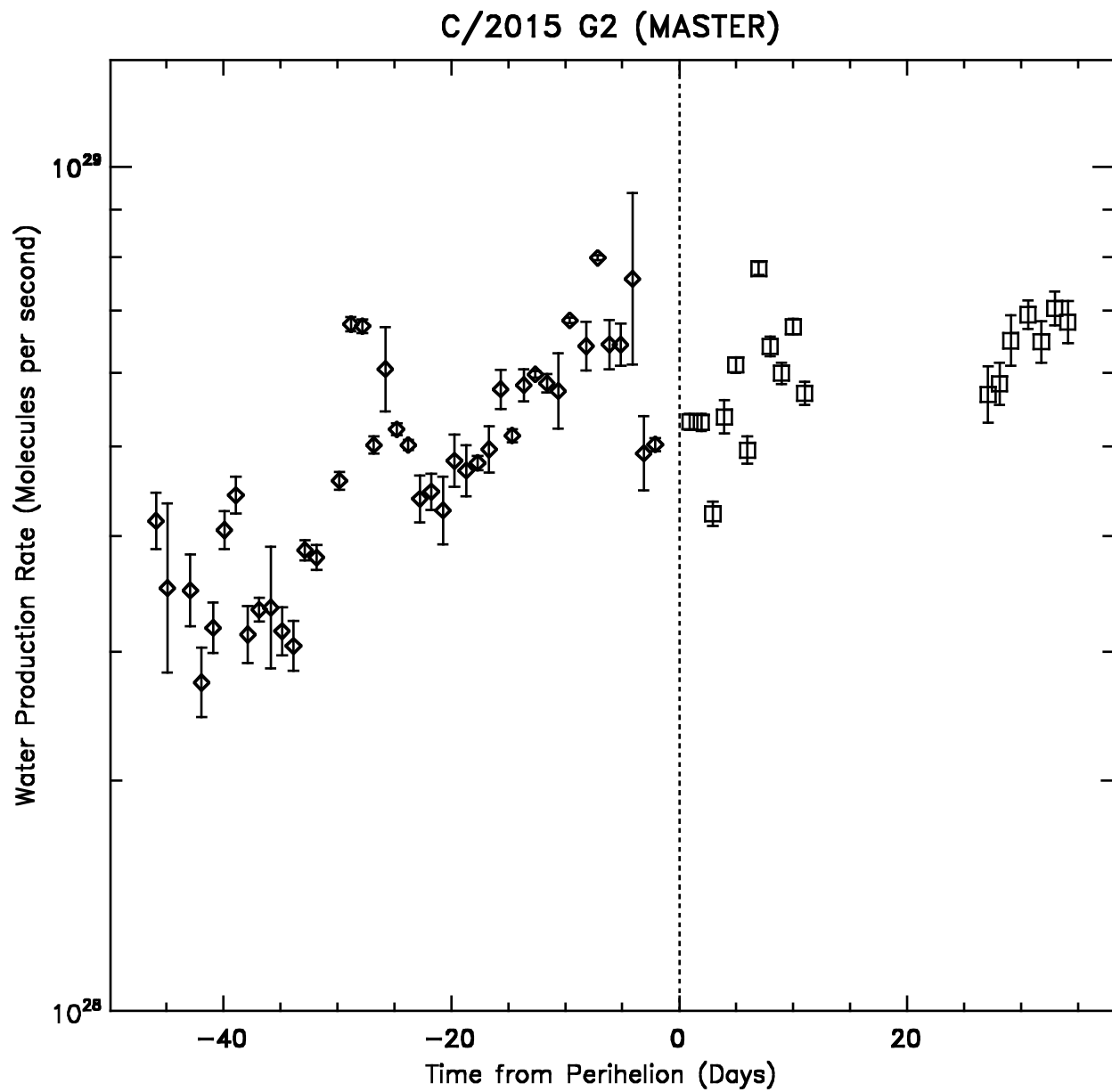


Fig. 7. Water production rate in comet C/2015 G2 (MASTER) over time in days from perihelion. The error bars correspond to the 1-sigma stochastic errors from noise in the data and the model fitting. The diamonds give the pre-perihelion values and the squares post-perihelion.

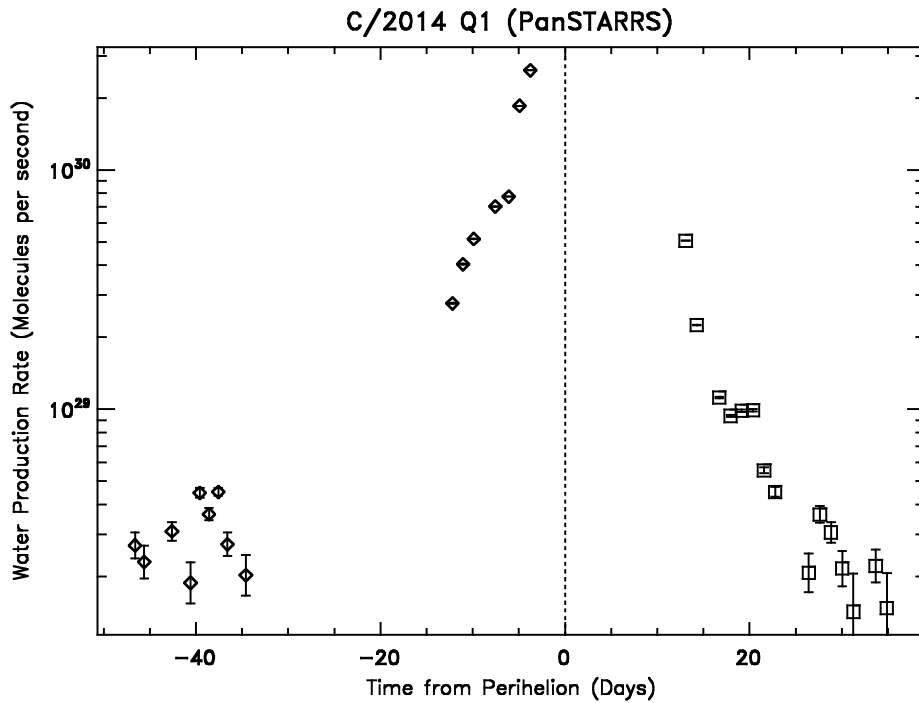


Fig. 8. Water production rate in comet C/2014 Q1 (PanSTARRS) over time in days from perihelion. The error bars correspond to the 1-sigma stochastic errors from noise in the data and the model fitting. The diamonds give the pre-perihelion values and the squares post-perihelion.

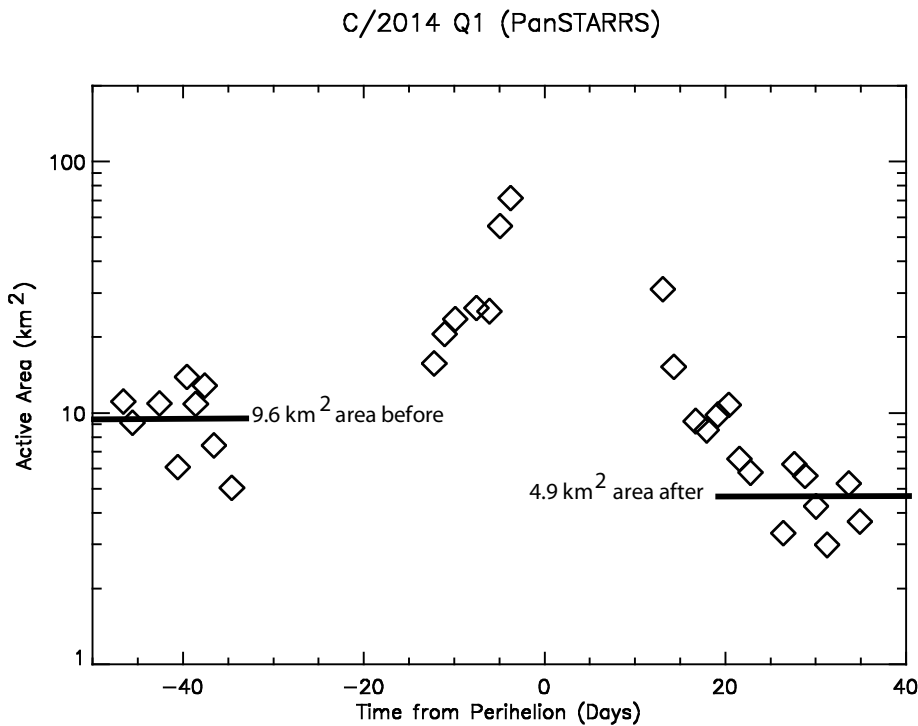


Fig. 9. Active area (km^2) in comet C/2014 Q1 (PanSTARRS) over time in days from perihelion. The horizontal line on the left shows the average active area before the enhanced perihelion peak and the horizontal line on the right shows the average active area after.

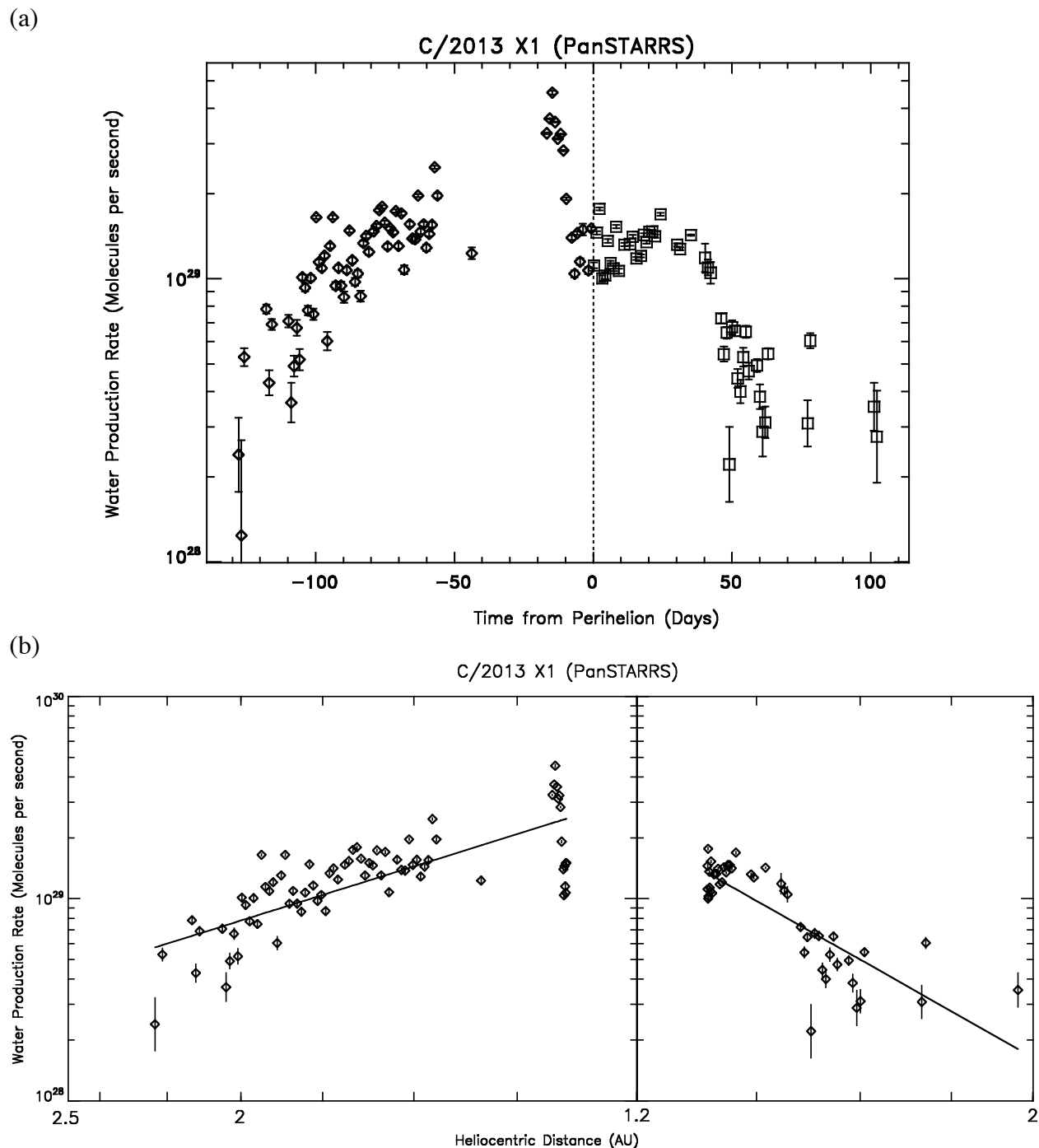


Fig. 10. Water production rate in comet C/2013 X1 (PanSTARRS). (a) Variation over time in days from perihelion. (b) Variation with heliocentric distance. The error bars correspond to the 1-sigma stochastic errors from noise in the data and the model fitting. The lines give the best-fit power-law variation with form given in Table 2.

Supplemental Tables

Table S1. SOHO/SWAN Observations of C/2012 K1 (PanSTARRS) and Water Production Rates

ΔT (days)	r (AU)	Δ (AU)	g (s ⁻¹)	Q (10 ²⁷ molecules s ⁻¹)	δQ (10 ²⁷ molecules s ⁻¹)
-126.088	2.197	1.515	0.002053	78.53	2.89
-125.088	2.185	1.509	0.002075	96.81	2.09
-124.088	2.173	1.503	0.002081	104.70	2.07
-117.065	2.090	1.481	0.002255	97.04	2.35
-116.065	2.078	1.481	0.002227	131.40	1.56
-115.056	2.066	1.481	0.002145	133.90	1.40
-114.056	2.054	1.482	0.002103	130.30	1.79
-113.056	2.042	1.483	0.002095	74.51	2.87
-112.056	2.031	1.485	0.002075	59.03	3.06
-111.037	2.018	1.487	0.002046	76.98	3.00
-110.037	2.007	1.490	0.002054	115.20	2.25
-109.037	1.995	1.493	0.002061	85.29	2.58
-108.027	1.983	1.497	0.002041	120.20	2.07
-107.027	1.971	1.502	0.002028	104.90	2.41
-105.026	1.947	1.512	0.001999	74.11	3.35
-104.009	1.935	1.518	0.002005	104.20	2.59
-103.009	1.924	1.524	0.001976	101.50	2.59
-102.009	1.912	1.531	0.001977	89.76	3.24
-100.997	1.900	1.538	0.002009	89.63	2.61
-99.996	1.888	1.545	0.002029	87.39	3.31
-98.997	1.876	1.553	0.002041	56.72	5.37
-97.996	1.865	1.561	0.002076	85.57	3.80
-96.982	1.853	1.570	0.002123	82.42	4.00
-95.982	1.841	1.579	0.002148	85.34	2.91
-94.982	1.829	1.588	0.002160	89.59	2.48
-91.967	1.794	1.617	0.002159	107.90	2.57
-90.966	1.782	1.627	0.002135	133.80	1.81
-89.953	1.771	1.638	0.002109	113.60	2.69
-88.954	1.759	1.648	0.002090	124.70	2.01
-87.954	1.747	1.659	0.002026	175.90	1.92
-86.954	1.736	1.670	0.002006	114.00	3.34
-85.937	1.724	1.681	0.002006	100.50	2.33
-84.937	1.712	1.692	0.002011	74.67	3.65
-83.937	1.701	1.703	0.001966	91.79	3.76
-82.925	1.689	1.714	0.001940	99.24	3.15
-81.925	1.678	1.726	0.001887	105.40	3.27
-80.925	1.666	1.737	0.001879	82.00	4.22

-79.926	1.655	1.749	0.001870	89.14	4.08
-78.908	1.643	1.760	0.001853	99.92	3.70
-77.907	1.632	1.772	0.001855	94.43	4.06
-76.907	1.621	1.783	0.001862	84.89	5.16
-75.907	1.610	1.795	0.001881	90.36	4.17
-73.897	1.587	1.818	0.002006	85.32	4.74
-72.898	1.576	1.829	0.002078	85.00	3.61
-71.898	1.565	1.840	0.002131	71.56	4.41
-69.878	1.542	1.863	0.002183	94.67	3.31
-68.878	1.531	1.874	0.002193	68.16	4.21
-67.878	1.520	1.885	0.002202	77.32	3.88
-66.878	1.509	1.896	0.002178	66.48	4.17
-65.878	1.499	1.906	0.002149	87.60	3.52
-64.676	1.486	1.919	0.002094	120.90	1.96
-63.676	1.475	1.929	0.002000	144.60	2.11
-62.676	1.464	1.940	0.001989	139.70	2.06
-61.676	1.454	1.950	0.001977	194.10	1.76
-60.698	1.443	1.959	0.001860	167.70	2.01
-59.698	1.433	1.969	0.001834	182.80	2.05
-58.698	1.422	1.978	0.001815	196.20	2.29
-56.698	1.402	1.997	0.001792	196.60	2.02
-55.698	1.392	2.005	0.001776	169.60	2.33
-53.704	1.372	2.022	0.001801	161.40	2.30
-52.704	1.362	2.030	0.001811	161.90	2.23
-51.704	1.352	2.038	0.001849	122.60	3.48
-50.704	1.342	2.045	0.002052	116.50	2.21
-49.704	1.332	2.053	0.002081	156.00	2.32
-47.727	1.314	2.066	0.002294	108.90	1.96
-46.727	1.304	2.072	0.002327	106.90	2.08
-45.728	1.295	2.079	0.002335	91.96	2.30
-2.794	1.056	1.976	0.001836	192.50	2.51
-1.817	1.055	1.964	0.001878	167.00	2.62
-0.818	1.055	1.952	0.001888	182.60	2.32
1.183	1.055	1.927	0.001897	151.70	1.91
2.183	1.055	1.914	0.001892	171.50	2.51
4.180	1.057	1.886	0.001883	151.30	2.92
6.180	1.060	1.857	0.001859	159.40	2.58
8.159	1.063	1.826	0.001792	137.30	2.68
9.159	1.066	1.811	0.001811	187.40	2.52
10.159	1.068	1.794	0.001839	139.20	2.89
11.159	1.071	1.778	0.001866	156.60	2.46
12.159	1.074	1.761	0.001874	155.90	3.64
13.153	1.077	1.744	0.001883	140.90	2.77

14.153	1.081	1.727	0.001883	163.60	2.56
15.153	1.085	1.709	0.001883	143.60	2.51
17.153	1.093	1.673	0.001890	149.20	3.80
18.133	1.097	1.655	0.001880	122.50	2.43
19.133	1.102	1.636	0.001878	120.50	2.57
20.133	1.107	1.617	0.001853	112.40	2.56
21.126	1.112	1.598	0.001862	130.40	2.38
22.126	1.117	1.579	0.001868	153.00	2.00
23.126	1.123	1.560	0.001860	134.50	2.13
24.126	1.128	1.540	0.001870	147.30	1.97
25.105	1.134	1.521	0.001873	114.10	2.22
34.383	1.198	1.335	0.002018	104.60	1.95
35.383	1.206	1.316	0.002033	118.90	1.07
36.383	1.214	1.296	0.002033	138.70	0.93
37.403	1.222	1.276	0.002004	139.30	0.92
38.403	1.231	1.257	0.001999	142.50	0.93
39.412	1.239	1.238	0.001920	118.80	6.79
41.431	1.256	1.200	0.001878	113.20	1.38
43.441	1.274	1.164	0.001875	107.50	1.89
45.459	1.292	1.129	0.001880	92.66	1.62
46.459	1.302	1.113	0.001878	92.63	1.56
47.471	1.311	1.097	0.001892	88.61	1.23
51.500	1.350	1.039	0.002138	69.77	1.28
52.516	1.360	1.026	0.002068	63.40	1.25
53.529	1.370	1.014	0.002096	75.38	1.11
62.618	1.464	0.952	0.001939	66.20	0.97
66.648	1.507	0.955	0.001956	100.50	0.66
67.649	1.518	0.959	0.001948	70.27	0.73
68.650	1.529	0.964	0.001945	55.91	0.96
69.651	1.540	0.970	0.001935	52.65	1.09
70.651	1.551	0.977	0.001943	48.53	1.05
71.810	1.564	0.987	0.002044	49.00	1.15
73.837	1.586	1.008	0.002175	42.54	1.14
74.837	1.597	1.020	0.002183	46.23	0.96
76.842	1.620	1.047	0.002187	46.35	0.91
77.864	1.632	1.063	0.002187	38.47	1.43
78.864	1.643	1.079	0.002175	50.98	0.88
79.871	1.654	1.096	0.002178	55.55	1.04
80.871	1.666	1.114	0.002169	54.03	1.65
81.892	1.678	1.133	0.002128	51.69	1.28
82.892	1.689	1.152	0.002076	48.03	1.81
83.901	1.701	1.172	0.002110	54.78	1.59
84.901	1.712	1.193	0.002158	36.38	2.21

85.920	1.724	1.215	0.002167	44.97	1.99
86.920	1.735	1.237	0.002162	61.65	1.02
87.931	1.747	1.260	0.002155	50.26	1.72
88.931	1.759	1.284	0.002109	51.01	1.40
90.948	1.782	1.332	0.002049	39.68	2.08
92.960	1.806	1.382	0.001983	25.92	4.15
93.960	1.817	1.408	0.001953	40.24	3.81
94.960	1.829	1.434	0.001932	36.78	2.85
95.976	1.841	1.461	0.001951	43.37	2.67
96.976	1.853	1.487	0.002105	31.04	3.32
97.989	1.865	1.515	0.002165	31.28	3.15
98.990	1.876	1.542	0.002192	34.20	2.65
99.989	1.888	1.569	0.002228	28.72	2.13
100.990	1.900	1.597	0.002227	28.58	3.54
102.004	1.912	1.625	0.002237	41.31	2.32

ΔT : Time from perihelion on 27.7 Aug 2014 UT in days

r : Heliocentric distance (AU)

Δ : Geocentric distance (AU)

g : Solar Lyman- α g-factor (photons s^{-1}) at 1 AU

Q : Daily-Average Water production rates (molecules s^{-1}) from the TRM

δQ : internal 1-sigma uncertainties

Table S2. SOHO/SWAN Observations of C/2013 US10 (Catalina) and Water Production Rates

ΔT (days)	r (AU)	Δ (AU)	g (s ⁻¹)	Q (10 ²⁷ molecules s ⁻¹)	δQ (10 ²⁷ molecules s ⁻¹)
-137.270	2.375	1.793	0.001572	54.62	22.07
-136.103	2.360	1.762	0.001837	43.59	16.22
-134.956	2.346	1.731	0.001934	30.63	20.19
-128.390	2.261	1.567	0.002192	73.97	7.48
-124.625	2.213	1.480	0.002129	75.54	7.28
-123.425	2.197	1.453	0.002099	92.04	6.27
-122.356	2.183	1.430	0.002086	52.13	10.83
-119.953	2.152	1.380	0.002038	64.94	7.95
-118.744	2.136	1.357	0.002007	108.00	6.06
-117.546	2.120	1.334	0.001972	99.28	5.11
-115.122	2.089	1.290	0.001906	74.93	6.41
-113.914	2.073	1.270	0.001880	68.61	13.35
-112.708	2.057	1.251	0.001840	64.09	7.00
-111.499	2.041	1.233	0.001841	79.63	5.71
-110.291	2.025	1.216	0.001851	121.20	12.85
-109.082	2.009	1.200	0.001941	121.00	9.00
-104.950	1.955	1.154	0.002065	158.90	2.15
-103.742	1.939	1.143	0.002065	126.20	5.42
-102.533	1.923	1.133	0.002070	95.80	8.21
-101.324	1.907	1.125	0.002067	138.50	2.84
-100.116	1.891	1.118	0.002063	94.46	4.37
-97.698	1.858	1.108	0.002010	123.40	3.91
-96.490	1.842	1.104	0.001992	116.30	4.03
-95.281	1.826	1.102	0.001975	131.20	4.02
-94.072	1.810	1.102	0.001966	118.90	4.17
-92.864	1.794	1.102	0.001930	122.30	4.55
-88.025	1.729	1.115	0.001859	100.60	3.75
-85.598	1.697	1.128	0.001918	131.70	9.55
-81.970	1.648	1.155	0.001955	112.70	15.17
-77.935	1.594	1.193	0.001968	133.70	6.60
-76.727	1.578	1.205	0.001954	122.20	4.94
-75.532	1.562	1.219	0.001959	142.60	5.72
-74.324	1.545	1.233	0.001949	104.10	9.00
-63.913	1.407	1.367	0.001834	190.70	26.81
-62.894	1.393	1.381	0.001856	147.20	4.33
-39.350	1.097	1.682	0.001705	325.20	4.27
-38.345	1.085	1.693	0.001719	224.70	6.14

-37.345	1.074	1.702	0.001742	228.60	5.23
-36.345	1.063	1.712	0.001751	241.10	4.49
-35.345	1.052	1.721	0.001785	296.90	2.74
-34.345	1.041	1.730	0.001815	277.20	4.17
-33.345	1.030	1.738	0.001849	288.90	3.75
-32.345	1.019	1.747	0.001895	191.60	5.23
-31.345	1.009	1.754	0.001957	233.80	4.19
-30.321	0.998	1.762	0.001984	211.10	4.75
-29.320	0.988	1.768	0.002002	217.00	4.89
-28.320	0.978	1.775	0.001984	275.70	4.12
-27.320	0.968	1.781	0.001961	286.50	4.18
-26.320	0.959	1.786	0.001930	256.30	4.79
-25.320	0.950	1.791	0.001898	432.20	3.80
14.739	0.869	1.526	0.001389	194.10	5.85
18.903	0.897	1.449	0.001675	175.90	4.38
19.904	0.904	1.430	0.001716	193.40	3.57
20.961	0.912	1.409	0.001765	204.80	3.67
22.732	0.927	1.373	0.001844	127.10	4.92
29.081	0.986	1.240	0.001812	168.70	3.92
30.065	0.996	1.218	0.001799	129.80	3.57
31.065	1.006	1.197	0.001815	169.90	2.79
32.057	1.016	1.175	0.001823	172.40	2.88
33.057	1.027	1.153	0.001830	152.80	3.37
34.037	1.037	1.132	0.001828	185.70	8.22
35.037	1.048	1.110	0.001808	185.10	2.33
36.037	1.059	1.088	0.001783	172.70	2.88
37.037	1.071	1.067	0.001785	132.10	3.21
38.027	1.082	1.046	0.001768	138.30	2.77
39.027	1.093	1.024	0.001750	160.40	2.56
40.009	1.105	1.004	0.001734	135.40	3.35
41.009	1.117	0.983	0.001721	150.90	2.61
41.998	1.128	0.963	0.001725	111.00	3.52
42.998	1.140	0.943	0.001717	160.20	2.48
43.981	1.152	0.923	0.001713	133.90	2.79
44.981	1.164	0.904	0.001726	124.40	2.73
45.969	1.176	0.886	0.001762	106.10	3.24
46.953	1.188	0.868	0.001814	96.99	4.44
47.953	1.201	0.851	0.001845	92.97	2.91
48.940	1.213	0.835	0.001892	91.23	2.55
49.924	1.226	0.819	0.001897	100.70	2.18
50.924	1.238	0.804	0.001902	91.12	2.26
51.910	1.251	0.790	0.001881	80.42	3.31
52.896	1.263	0.778	0.001867	94.31	4.46

53.881	1.276	0.766	0.001840	102.50	1.93
54.881	1.289	0.755	0.001833	105.10	2.09
55.868	1.302	0.746	0.001827	117.50	7.83
56.852	1.314	0.738	0.001825	114.70	4.68
57.840	1.327	0.731	0.001823	112.40	1.80
58.840	1.340	0.726	0.001827	115.00	1.72
61.813	1.379	0.719	0.001810	114.50	2.25
62.792	1.392	0.720	0.001793	83.31	2.08
63.792	1.405	0.722	0.001807	95.38	1.79
64.786	1.418	0.726	0.001805	91.51	4.40
65.786	1.432	0.732	0.001800	98.07	1.68
66.787	1.445	0.739	0.001792	85.44	1.83
67.761	1.458	0.748	0.001791	78.61	1.81
69.760	1.484	0.769	0.001767	78.35	1.94
70.458	1.494	0.778	0.001792	83.43	1.96
71.459	1.507	0.792	0.001830	70.56	2.09
72.459	1.521	0.807	0.001874	68.51	2.10
73.460	1.534	0.823	0.001919	62.97	1.71
74.456	1.547	0.841	0.001927	65.18	2.96
75.456	1.561	0.859	0.001946	62.37	4.80
76.432	1.574	0.878	0.001925	67.86	7.14
78.160	1.597	0.914	0.001911	78.38	2.44
79.153	1.610	0.936	0.001918	70.81	2.40
80.153	1.624	0.959	0.001902	64.89	3.20
81.132	1.637	0.982	0.001867	59.80	3.13
82.132	1.650	1.006	0.001855	66.73	2.82
83.132	1.664	1.031	0.001849	70.83	9.14
84.124	1.677	1.056	0.001850	63.77	6.47
85.124	1.690	1.081	0.001823	79.33	8.16
86.124	1.704	1.108	0.001817	51.42	6.89
87.105	1.717	1.134	0.001793	68.66	9.81
88.105	1.730	1.161	0.001799	63.98	8.79
89.105	1.744	1.189	0.001803	59.62	4.12
90.094	1.757	1.216	0.001800	47.50	5.23
91.094	1.770	1.244	0.001791	63.86	12.19
92.077	1.783	1.272	0.001803	64.22	6.63
93.077	1.797	1.301	0.001796	51.95	12.27
94.077	1.810	1.330	0.001777	31.20	8.13
95.077	1.823	1.359	0.001773	40.32	10.33

ΔT : Time from perihelion on 15.7 Nov 2015 UT in days

r : Heliocentric distance (AU)

Δ : Geocentric distance (AU)

g: Solar Lyman- α g-factor (photons s^{-1}) at 1 AU
Q: Daily-Average Water production rates (molecules s^{-1}) from the TRM
 δQ : internal 1-sigma uncertainties

Table S3. SOHO/SWAN Observations of C/2013 V5 (Oukaimeden) and Water Production Rates

ΔT (days)	r (AU)	Δ (AU)	g (s ⁻¹)	Q (10 ²⁷ molecules s ⁻¹)	δQ (10 ²⁷ molecules s ⁻¹)
-38.435	1.010	1.230	0.002013	42.12	4.06
-35.435	0.965	1.122	0.002109	32.13	6.07
-34.444	0.951	1.087	0.002161	41.18	5.75
-33.444	0.936	1.051	0.002156	35.31	7.22
-32.444	0.922	1.014	0.002155	37.72	8.08
-30.464	0.894	0.943	0.002171	40.85	5.02
-29.464	0.880	0.907	0.002159	34.78	6.29
-26.472	0.839	0.802	0.002193	38.01	4.39
-25.493	0.826	0.769	0.002067	41.28	3.16
-24.493	0.813	0.735	0.002022	45.84	7.71
-23.493	0.800	0.702	0.002004	40.35	5.04
-22.501	0.788	0.671	0.001995	37.75	3.36
-21.501	0.775	0.640	0.002028	40.36	2.54
-20.522	0.764	0.612	0.002057	45.15	3.39
-19.522	0.752	0.585	0.002045	48.81	3.03
-18.529	0.741	0.560	0.002042	45.23	4.50
-17.529	0.730	0.537	0.002038	44.98	2.92
-16.552	0.719	0.517	0.002021	45.48	3.10
-14.553	0.700	0.488	0.001951	47.62	2.94
-13.553	0.690	0.479	0.001916	45.35	3.36
-12.554	0.682	0.474	0.001884	56.73	3.16
-11.554	0.673	0.474	0.001855	46.49	3.51
-11.172	0.670	0.475	0.001858	43.46	3.24
-10.171	0.663	0.481	0.001860	44.01	3.47
-9.173	0.656	0.491	0.001835	44.07	4.99
-8.199	0.650	0.505	0.001840	45.36	5.38
-7.202	0.645	0.523	0.001825	47.30	2.75
-6.227	0.640	0.544	0.001815	46.38	4.93
-4.456	0.633	0.589	0.001832	61.02	2.34
-3.432	0.630	0.619	0.001850	53.26	1.81
-2.432	0.628	0.649	0.001869	50.47	2.77
-0.404	0.626	0.716	0.001872	64.37	3.39
0.596	0.626	0.750	0.001869	74.47	2.84
2.602	0.628	0.823	0.001846	54.94	3.33
3.620	0.630	0.859	0.001839	66.71	3.40
4.620	0.633	0.896	0.001848	63.88	3.73
5.622	0.637	0.933	0.001878	38.98	5.57

6.622	0.642	0.970	0.001898	40.55	6.02
8.634	0.653	1.044	0.001878	40.39	6.52
9.633	0.659	1.081	0.001872	36.78	6.12
10.633	0.666	1.117	0.001898	32.90	6.10

ΔT : Time from perihelion on 28.2 Sep 2014 UT in days

r : Heliocentric distance (AU)

Δ : Geocentric distance (AU)

g : Solar Lyman- α g-factor (photons s^{-1}) at 1 AU

Q : Daily-Average Water production rates (molecules s^{-1}) from the TRM

δQ : internal 1-sigma uncertainties

Table S4. SOHO/SWAN Observations of C/2013 R1 (Lovejoy) and Water Production Rates

ΔT (days)	r (AU)	Δ (AU)	g (s ⁻¹)	Q (10 ²⁷ molecules s ⁻¹)	δQ (10 ²⁷ molecules s ⁻¹)
-69.730	1.482	1.030	0.001760	15.83	6.94
-68.730	1.468	1.006	0.001707	33.01	3.33
-67.730	1.455	0.982	0.001689	42.92	1.77
-66.743	1.442	0.959	0.001688	12.09	9.60
-65.743	1.428	0.935	0.001688	39.04	2.99
-64.743	1.415	0.911	0.001751	35.75	3.31
-63.743	1.401	0.888	0.001799	49.29	1.78
-62.743	1.388	0.865	0.001899	43.78	2.38
-61.758	1.375	0.842	0.001942	39.59	1.69
-60.758	1.362	0.819	0.001918	43.32	1.54
-59.758	1.349	0.796	0.001899	38.72	2.09
-58.772	1.336	0.774	0.001883	49.09	1.50
-57.771	1.322	0.752	0.001913	50.64	1.41
-56.772	1.309	0.729	0.001859	44.75	2.76
-54.787	1.283	0.686	0.001850	34.18	1.80
-53.800	1.271	0.665	0.001849	48.36	1.60
-52.800	1.258	0.644	0.001900	34.44	1.61
-51.800	1.245	0.623	0.001885	47.74	4.65
-50.812	1.232	0.603	0.001884	38.32	3.08
-49.858	1.220	0.584	0.001943	37.93	2.01
-48.857	1.207	0.565	0.001911	48.55	1.01
-46.857	1.182	0.528	0.001866	43.46	1.08
-45.858	1.170	0.510	0.001850	51.17	0.86
-44.837	1.157	0.493	0.001738	80.59	1.17
-43.851	1.145	0.478	0.001797	53.57	0.75
-42.838	1.133	0.463	0.001840	63.79	0.62
-41.831	1.120	0.449	0.001819	63.61	0.60
-40.818	1.108	0.436	0.001858	58.78	0.63
-39.804	1.096	0.424	0.001886	46.14	1.29
-38.789	1.084	0.414	0.001913	42.42	1.38
-37.761	1.072	0.405	0.001949	43.93	1.21
-36.746	1.061	0.398	0.001885	53.92	1.07
-35.996	1.052	0.394	0.001904	58.72	0.97
-34.981	1.041	0.389	0.001839	68.81	1.09
-33.967	1.029	0.387	0.001775	61.00	1.08
-32.952	1.018	0.386	0.001753	70.56	1.04
-30.910	0.997	0.390	0.001721	78.92	1.06

-29.894	0.986	0.395	0.001670	84.07	0.82
-28.882	0.976	0.401	0.001647	89.85	0.92
-27.864	0.965	0.409	0.001642	89.45	0.99
-26.864	0.956	0.418	0.001613	94.64	0.94
-25.854	0.946	0.428	0.001640	86.99	1.00
-24.835	0.937	0.440	0.001651	89.64	0.83
-22.835	0.919	0.467	0.001683	82.26	1.04
-21.826	0.910	0.482	0.001664	87.50	1.00
-20.827	0.902	0.498	0.001649	87.77	1.08
-19.827	0.894	0.514	0.001631	95.34	1.00
-18.827	0.886	0.531	0.001655	95.06	0.98
-17.827	0.879	0.549	0.001637	97.92	1.06
-16.827	0.872	0.567	0.001639	122.10	0.94
-15.828	0.865	0.585	0.001689	115.70	1.06
-14.828	0.859	0.604	0.001715	105.20	1.16
-13.828	0.853	0.623	0.001737	102.40	1.08
-12.828	0.847	0.642	0.001763	94.61	1.18
-11.828	0.842	0.662	0.001757	108.80	1.13
-10.832	0.837	0.682	0.001752	130.40	1.03
-9.832	0.833	0.702	0.001769	118.00	1.06
-8.832	0.829	0.722	0.001763	116.10	1.10
-7.832	0.825	0.742	0.001765	119.60	1.23
-6.832	0.822	0.762	0.001697	135.60	1.13
-5.832	0.819	0.782	0.001692	110.50	1.49
-4.857	0.817	0.801	0.001598	120.50	1.66
-3.857	0.815	0.822	0.001548	155.10	1.37
-2.857	0.813	0.842	0.001501	140.20	1.83
-1.857	0.812	0.861	0.001497	113.10	2.24
-0.860	0.812	0.881	0.001511	148.20	1.57
0.140	0.812	0.901	0.001509	143.50	1.80
1.140	0.812	0.920	0.001465	137.10	1.93
2.140	0.813	0.940	0.001526	142.20	1.75
3.140	0.814	0.959	0.001541	142.50	2.03
4.114	0.815	0.977	0.001510	132.90	1.92
5.114	0.817	0.996	0.001528	113.30	1.91
6.114	0.820	1.015	0.001513	129.10	2.19
7.114	0.823	1.033	0.001514	122.30	1.90
8.115	0.826	1.051	0.001595	106.90	2.16
10.111	0.834	1.086	0.001549	149.00	1.81
11.111	0.839	1.103	0.001579	116.00	1.97
12.111	0.844	1.120	0.001640	107.90	4.02
13.111	0.849	1.137	0.001694	107.00	2.84
14.111	0.855	1.153	0.001737	87.55	1.51

15.953	0.866	1.182	0.001793	113.70	1.11
17.953	0.880	1.213	0.001689	120.60	3.78
18.953	0.887	1.228	0.001691	98.35	10.45
19.914	0.895	1.242	0.001651	110.60	1.44
20.914	0.903	1.256	0.001674	90.16	1.56
21.918	0.911	1.270	0.001623	91.10	1.82
22.918	0.919	1.283	0.001616	94.05	1.79
23.918	0.928	1.297	0.001652	105.90	1.70
24.918	0.937	1.310	0.001643	89.32	2.45
25.918	0.947	1.322	0.001685	96.26	7.16
26.918	0.956	1.334	0.001748	81.53	3.20
27.942	0.966	1.346	0.001809	106.50	1.44
28.942	0.976	1.358	0.001778	82.99	1.47
29.942	0.986	1.369	0.001758	81.76	1.56
30.942	0.997	1.380	0.001685	109.50	1.73
31.942	1.007	1.390	0.001710	100.80	1.70
32.942	1.018	1.401	0.001755	79.03	1.90
33.942	1.029	1.410	0.001749	74.79	1.64
34.948	1.040	1.420	0.001704	72.52	1.75
35.948	1.052	1.429	0.001737	71.76	2.18
36.948	1.063	1.438	0.001732	90.68	1.56
37.948	1.074	1.447	0.001745	78.60	1.76
38.948	1.086	1.455	0.001732	54.66	2.41
39.948	1.098	1.463	0.001736	68.03	2.39
40.948	1.110	1.470	0.001713	72.19	1.96
41.970	1.122	1.478	0.001700	86.79	11.55
42.970	1.134	1.485	0.001585	58.86	3.14
43.970	1.146	1.492	0.001613	100.20	1.45
44.970	1.159	1.498	0.001610	81.98	2.55
45.970	1.171	1.504	0.001585	99.30	2.20
46.970	1.184	1.510	0.001603	90.95	2.04
47.970	1.196	1.515	0.001571	114.30	1.44
48.970	1.209	1.521	0.001648	110.20	1.37
49.970	1.221	1.526	0.001717	73.21	1.80
51.978	1.247	1.535	0.001790	70.77	1.66
52.978	1.260	1.539	0.001777	107.60	1.18
53.978	1.273	1.543	0.001777	66.95	2.06
55.978	1.299	1.550	0.001838	55.46	2.19
56.978	1.312	1.553	0.001891	24.11	4.50
57.978	1.325	1.556	0.001897	44.56	2.59
58.978	1.338	1.558	0.001957	49.55	2.15
59.998	1.352	1.561	0.001937	41.43	2.95
60.998	1.365	1.563	0.001931	47.43	2.32

61.998	1.378	1.564	0.001930	44.05	2.67
63.998	1.405	1.568	0.001905	46.93	2.01
64.998	1.418	1.569	0.001884	41.02	2.06
65.998	1.432	1.570	0.001842	74.45	1.73
66.998	1.445	1.570	0.001743	65.56	1.99
67.998	1.458	1.571	0.001747	70.66	5.60
68.998	1.472	1.571	0.001753	56.96	2.42
69.998	1.485	1.572	0.001743	63.26	8.48
71.008	1.499	1.571	0.001725	58.32	1.66
72.008	1.512	1.571	0.001781	67.84	6.00
73.008	1.526	1.571	0.001785	48.00	2.54
75.008	1.553	1.570	0.001771	60.29	4.08
77.009	1.579	1.568	0.001847	29.00	2.90
78.009	1.593	1.566	0.001840	64.99	1.95
79.009	1.606	1.565	0.001863	35.03	2.20
80.025	1.620	1.563	0.001925	60.28	10.85
81.025	1.634	1.562	0.001908	32.12	5.93
82.025	1.647	1.560	0.001940	25.89	4.29
83.025	1.661	1.558	0.001940	58.86	1.87
84.025	1.674	1.556	0.001949	27.05	4.12
85.025	1.688	1.554	0.001938	21.05	4.93
86.025	1.701	1.551	0.001928	36.62	3.01
87.025	1.714	1.549	0.001881	8.47	12.28
91.039	1.768	1.539	0.001745	54.90	3.00

ΔT : Time from perihelion on 22.7 Dec 2013 UT in days

r : Heliocentric distance (AU)

Δ : Geocentric distance (AU)

g : Solar Lyman- α g-factor (photons s^{-1}) at 1 AU

Q : Daily-Average Water production rates (molecules s^{-1}) from the TRM

δQ : internal 1-sigma uncertainties

Table S5. SOHO/SWAN Observations of C/2014 E2 (Jacques) and Water Production Rates

ΔT (days)	r (AU)	Δ (AU)	g (s ⁻¹)	Q (10 ²⁷ molecules s ⁻¹)	δQ (10 ²⁷ molecules s ⁻¹)
-88.844	1.763	0.972	0.002045	22.12	4.00
-87.844	1.748	0.972	0.002026	36.63	2.53
-86.822	1.734	0.973	0.002033	48.78	1.83
-85.843	1.719	0.974	0.002025	47.77	2.17
-84.822	1.705	0.976	0.002049	55.22	1.85
-81.823	1.661	0.988	0.001930	42.25	2.71
-80.813	1.646	0.994	0.001914	24.53	4.80
-79.813	1.631	1.001	0.001891	37.91	2.90
-78.812	1.617	1.008	0.001859	50.31	2.60
-77.812	1.602	1.016	0.001804	48.48	2.61
-76.812	1.587	1.024	0.001808	62.30	2.09
-75.795	1.572	1.034	0.001731	82.73	1.81
-74.795	1.558	1.044	0.001699	77.31	2.09
-73.795	1.543	1.054	0.001732	49.97	3.33
-72.796	1.528	1.065	0.001684	48.33	2.97
-71.782	1.513	1.076	0.001694	79.70	1.97
-70.782	1.498	1.088	0.001715	75.42	1.93
-69.782	1.483	1.100	0.001741	80.70	2.15
-68.782	1.469	1.113	0.001762	60.67	2.37
-67.782	1.454	1.126	0.001851	45.29	3.03
-65.768	1.424	1.153	0.001887	41.02	2.27
-64.768	1.409	1.167	0.002036	42.27	2.76
-63.752	1.394	1.181	0.001990	41.61	3.50
-62.752	1.379	1.195	0.001946	63.33	2.00
-61.752	1.364	1.209	0.001932	69.69	1.97
-60.752	1.349	1.224	0.001925	67.16	1.31
-59.751	1.334	1.238	0.001908	62.70	6.97
-58.740	1.319	1.253	0.001852	78.61	4.13
-57.751	1.304	1.268	0.001882	71.68	3.07
-56.741	1.289	1.283	0.001856	87.54	2.26
-55.741	1.274	1.298	0.001853	78.10	2.91
-53.741	1.245	1.327	0.001870	105.40	2.27
-52.722	1.229	1.342	0.001869	93.49	2.12
-51.721	1.214	1.357	0.001858	89.01	2.63
-50.721	1.200	1.371	0.001752	63.25	3.77
-48.721	1.170	1.400	0.001808	69.89	2.88
-47.721	1.155	1.414	0.001872	73.58	2.84

-29.686	0.900	1.626	0.001714	134.70	4.58
-28.686	0.887	1.634	0.001770	287.40	2.20
-27.686	0.874	1.642	0.001721	286.00	25.63
-26.686	0.862	1.650	0.001722	201.00	43.38
-25.686	0.849	1.657	0.001685	246.60	24.63
-24.686	0.837	1.663	0.001696	261.40	73.46
10.346	0.699	1.455	0.001837	244.30	2.03
11.347	0.705	1.436	0.001946	212.20	1.77
12.347	0.713	1.417	0.001870	166.60	2.26
13.347	0.720	1.397	0.001852	183.70	12.20
21.338	0.798	1.222	0.001504	207.70	22.89
22.335	0.809	1.199	0.001518	171.00	14.01
23.335	0.821	1.175	0.001526	174.20	25.07
27.319	0.870	1.080	0.001581	106.10	3.09
29.311	0.895	1.031	0.001659	89.84	2.83
30.311	0.908	1.007	0.001785	110.60	3.34
31.310	0.922	0.982	0.001850	131.60	0.97
32.291	0.935	0.958	0.001929	127.50	1.37
33.291	0.948	0.934	0.001958	120.90	7.49
34.281	0.962	0.910	0.001946	90.49	1.12
37.262	1.004	0.840	0.001773	141.40	0.78
38.263	1.018	0.817	0.001753	157.40	0.89
39.252	1.032	0.794	0.001686	115.10	1.04
40.234	1.046	0.772	0.001626	125.50	1.20
41.223	1.060	0.751	0.001570	132.70	2.29
42.223	1.075	0.730	0.001547	112.40	1.11
43.206	1.089	0.710	0.001541	94.77	1.19
48.150	1.162	0.624	0.001420	120.70	0.92
52.093	1.220	0.578	0.001612	71.48	1.29
53.077	1.235	0.570	0.001703	82.78	1.09
54.066	1.249	0.565	0.001643	89.74	1.29
58.039	1.309	0.562	0.001803	52.89	1.08
59.040	1.324	0.566	0.001803	53.57	0.91
60.015	1.338	0.573	0.001863	54.90	0.79
61.015	1.353	0.581	0.001855	52.90	1.02
68.681	1.467	0.701	0.001533	111.40	2.32
69.658	1.482	0.722	0.001533	59.77	3.53
70.658	1.496	0.745	0.001533	66.29	4.69
72.651	1.526	0.792	0.001533	75.20	2.03
73.630	1.540	0.817	0.001533	57.31	2.98
74.630	1.555	0.843	0.001533	71.19	2.75
75.622	1.570	0.869	0.001533	25.85	4.96
76.621	1.585	0.896	0.001533	72.58	1.90

77.602	1.599	0.923	0.001533	86.93	3.55
78.602	1.614	0.951	0.001533	77.01	9.80
79.592	1.628	0.979	0.001533	66.03	2.70
80.592	1.643	1.008	0.001533	39.71	4.42
81.592	1.657	1.038	0.001533	34.31	5.91
83.155	1.680	1.084	0.001533	23.49	8.76
84.156	1.695	1.114	0.001532	63.88	3.95
86.167	1.724	1.175	0.001532	42.59	6.10
87.167	1.739	1.206	0.001532	16.28	14.43
95.196	1.854	1.460	0.001519	32.86	8.20
96.196	1.869	1.492	0.001518	60.33	5.40
97.196	1.883	1.524	0.001518	76.36	4.60
98.196	1.897	1.556	0.001518	25.66	11.01
102.212	1.954	1.685	0.001518	41.16	7.89
104.212	1.982	1.750	0.001518	34.62	10.75
105.212	1.996	1.782	0.001518	47.01	7.50
110.226	2.066	1.943	0.001518	28.20	13.81

ΔT : Time from perihelion on 2.5 Jul 2013 UT in days

r : Heliocentric distance (AU)

Δ : Geocentric distance (AU)

g : Solar Lyman- α g-factor (photons s^{-1}) at 1 AU

Q : Daily-Average Water production rates (molecules s^{-1}) from the TRM

δQ : internal 1-sigma uncertainties

Table S6. SOHO/SWAN Observations of C/2014 Q2 (Lovejoy) and Water Production Rates

ΔT (days)	r (AU)	Δ (AU)	g (s ⁻¹)	Q (10 ²⁷ molecules s ⁻¹)	δQ (10 ²⁷ molecules s ⁻¹)
-61.833	1.583	1.079	0.001901	160.70	0.86
-59.832	1.567	1.037	0.001898	208.40	0.78
-56.832	1.543	0.974	0.002050	112.70	0.87
-54.832	1.527	0.932	0.001450	123.20	1.52
-51.853	1.505	0.871	0.002164	180.50	0.44
-41.494	1.432	0.673	0.001891	239.00	6.37
-40.494	1.426	0.656	0.001873	211.30	0.59
-38.853	1.416	0.628	0.001422	177.90	14.73
-36.881	1.404	0.598	0.001818	216.00	8.85
-35.881	1.398	0.584	0.001823	225.20	0.50
-34.883	1.393	0.570	0.001832	237.80	0.42
-33.883	1.387	0.557	0.001829	235.30	0.39
-32.909	1.382	0.546	0.001840	237.10	0.41
-31.913	1.377	0.535	0.001872	232.70	0.36
-30.937	1.372	0.525	0.001887	235.60	0.47
-29.937	1.367	0.516	0.001934	231.20	6.60
-28.942	1.362	0.508	0.001986	232.70	0.37
-27.971	1.357	0.502	0.002013	280.70	0.31
-26.971	1.353	0.496	0.002031	263.90	0.34
-25.994	1.349	0.492	0.002033	274.70	0.37
-25.000	1.344	0.489	0.002104	254.20	0.37
-24.021	1.340	0.487	0.002010	291.40	0.36
-23.029	1.336	0.487	0.001988	287.20	0.37
-22.050	1.333	0.488	0.001953	311.60	0.34
-21.079	1.329	0.490	0.001951	317.00	0.39
-20.087	1.326	0.494	0.001909	351.80	0.28
-19.107	1.322	0.498	0.001870	356.10	0.31
-18.116	1.319	0.504	0.001831	400.70	0.35
-17.133	1.316	0.511	0.001787	439.70	0.33
-16.137	1.313	0.519	0.001765	457.30	0.34
-15.153	1.311	0.529	0.001752	479.90	0.34
-14.157	1.308	0.539	0.001734	436.70	0.53
-9.113	1.298	0.603	0.001801	494.60	0.26
-6.088	1.294	0.650	0.001865	493.70	4.54
-5.071	1.293	0.667	0.001886	483.10	0.23
-3.059	1.291	0.701	0.001952	564.60	0.21
-2.059	1.291	0.718	0.001973	660.80	0.18

-1.043	1.291	0.737	0.001977	562.10	41.82
1.970	1.291	0.792	0.001972	570.00	54.26
2.985	1.291	0.811	0.001958	561.30	29.55
3.985	1.292	0.829	0.001940	591.40	68.05
6.000	1.294	0.868	0.001885	629.10	56.08
7.000	1.295	0.887	0.001833	656.30	62.83
8.000	1.296	0.906	0.001789	759.10	58.71
9.014	1.298	0.925	0.001763	789.10	63.31
17.042	1.316	1.078	0.001839	774.50	195.80
18.042	1.319	1.097	0.001794	809.60	147.70
19.042	1.322	1.116	0.001811	649.20	75.18
20.042	1.325	1.134	0.001836	883.60	124.70
21.059	1.329	1.153	0.001834	867.70	146.80
22.059	1.333	1.172	0.001857	868.70	80.13
23.059	1.337	1.190	0.001871	705.90	63.99
24.059	1.340	1.209	0.001872	757.30	89.22
25.059	1.345	1.227	0.001880	686.10	62.88
26.070	1.349	1.245	0.001892	624.50	41.28
27.070	1.353	1.263	0.001886	633.10	20.39
28.070	1.358	1.281	0.001878	601.20	8.96
29.070	1.363	1.299	0.001861	643.30	2.61
30.070	1.368	1.316	0.001860	670.40	0.25
31.070	1.373	1.333	0.001840	571.50	0.34
32.088	1.378	1.351	0.001836	586.40	0.27
33.088	1.383	1.368	0.001812	598.50	0.28
35.088	1.394	1.402	0.001754	554.30	0.36
36.088	1.400	1.419	0.001726	635.00	0.35
37.088	1.405	1.435	0.001701	565.10	0.35
38.098	1.411	1.451	0.001696	638.20	0.35
47.572	1.473	1.598	0.001391	456.80	0.72
48.572	1.481	1.612	0.001391	633.50	0.77
49.572	1.488	1.627	0.001391	508.70	0.72
50.572	1.495	1.641	0.001391	521.50	0.85
51.572	1.502	1.655	0.001391	547.50	0.72
52.572	1.510	1.669	0.001400	533.20	0.95
53.564	1.517	1.682	0.001400	614.40	0.62
54.564	1.525	1.696	0.001400	527.00	0.83
55.564	1.533	1.709	0.001400	528.00	0.77
56.564	1.541	1.722	0.001400	504.30	0.90
58.564	1.557	1.748	0.001400	437.50	1.12
59.564	1.565	1.761	0.001408	397.70	1.07
60.564	1.573	1.773	0.001408	440.40	0.89
61.543	1.581	1.785	0.001408	506.80	0.81

62.543	1.589	1.797	0.001408	431.20	17.66
64.543	1.606	1.821	0.001408	422.20	8.24
65.543	1.615	1.833	0.001408	363.90	17.36
66.543	1.623	1.845	0.001408	388.00	11.86
67.543	1.632	1.856	0.001417	417.10	0.88
68.543	1.641	1.867	0.001881	287.70	10.94
69.543	1.649	1.878	0.001929	297.00	13.22
70.536	1.658	1.889	0.001971	315.30	6.79
71.537	1.667	1.900	0.002014	293.20	17.21
72.536	1.676	1.910	0.002045	346.50	0.67
73.537	1.685	1.921	0.002033	323.70	0.73
74.536	1.694	1.931	0.001996	306.70	0.70
75.537	1.703	1.941	0.001960	347.90	0.72
76.537	1.713	1.951	0.001923	299.10	0.80
77.537	1.722	1.961	0.001895	269.00	0.84
78.537	1.731	1.971	0.001879	295.00	0.85
79.514	1.740	1.980	0.001854	251.80	0.93
80.514	1.750	1.989	0.001833	249.60	0.93
81.514	1.759	1.999	0.001842	256.30	0.90
82.513	1.769	2.008	0.001845	294.40	0.69
84.513	1.788	2.026	0.001848	230.60	0.92
85.514	1.797	2.035	0.001861	268.10	0.80
86.513	1.807	2.043	0.001863	219.30	0.86
87.513	1.817	2.052	0.001861	211.40	0.86
89.508	1.836	2.069	0.001874	213.20	0.96
90.508	1.846	2.077	0.001874	195.20	1.06
91.508	1.856	2.085	0.001902	206.50	0.94
92.508	1.865	2.093	0.001917	194.70	0.94
93.509	1.875	2.101	0.001962	221.00	0.87
94.509	1.885	2.109	0.001980	184.70	0.96
95.509	1.895	2.117	0.002002	187.90	0.89
96.484	1.905	2.125	0.002007	231.40	0.79
97.484	1.915	2.132	0.002002	279.70	0.69
98.484	1.925	2.140	0.001985	239.10	0.73
99.484	1.935	2.147	0.001959	237.70	0.75
100.484	1.945	2.155	0.001918	256.60	0.77
101.484	1.955	2.162	0.001874	218.20	0.87
102.484	1.965	2.169	0.001846	253.30	0.84
103.484	1.976	2.177	0.001808	264.80	0.83
104.484	1.986	2.184	0.001782	200.90	1.07
105.480	1.996	2.191	0.001762	227.50	1.02
106.480	2.006	2.198	0.001763	221.20	1.02
107.480	2.016	2.205	0.001770	172.30	1.23

108.480	2.027	2.212	0.001770	186.70	1.11
109.480	2.037	2.219	0.001808	167.50	1.30
110.480	2.047	2.226	0.002007	138.50	1.22
111.480	2.058	2.232	0.001826	128.20	1.46
112.480	2.068	2.239	0.001840	147.10	1.42
113.456	2.078	2.246	0.001868	130.60	1.41
114.456	2.089	2.253	0.001876	139.30	1.26
115.456	2.099	2.259	0.001908	153.50	1.31
116.456	2.109	2.266	0.001937	118.30	1.43
117.456	2.120	2.273	0.001957	130.50	1.35
118.456	2.130	2.280	0.001969	136.20	1.22
119.456	2.141	2.286	0.001989	121.60	1.29
120.456	2.151	2.293	0.001990	132.00	1.20
121.456	2.162	2.300	0.001988	146.80	1.15
122.456	2.172	2.307	0.001964	139.40	1.13

ΔT : Time from perihelion on 30.1 Jan 2015 UT in days

r : Heliocentric distance (AU)

Δ : Geocentric distance (AU)

g : Solar Lyman- α g-factor (photons s^{-1}) at 1 AU

Q : Daily-Average Water production rates (molecules s^{-1}) from the TRM

δQ : internal 1-sigma uncertainties

Table S7. SOHO/SWAN Observations of C/2015 G2 (MASTER) and Water Production Rates

ΔT (days)	r (AU)	Δ (AU)	g (s ⁻¹)	Q (10 ²⁷ molecules s ⁻¹)	δQ (10 ²⁷ molecules s ⁻¹)
-45.896	1.159	1.464	0.002247	41.54	3.03
-44.896	1.146	1.430	0.001572	35.16	8.20
-42.895	1.121	1.363	0.002174	34.95	3.25
-41.895	1.108	1.329	0.002139	27.81	2.50
-40.895	1.096	1.295	0.002116	31.87	2.05
-39.895	1.083	1.261	0.002085	40.61	1.94
-38.895	1.071	1.227	0.002064	44.29	2.07
-37.843	1.058	1.191	0.002053	31.33	2.30
-36.843	1.046	1.156	0.002047	33.31	1.00
-35.843	1.034	1.122	0.001540	33.50	5.48
-34.837	1.022	1.087	0.001540	31.59	1.96
-33.838	1.011	1.052	0.002024	30.46	1.95
-32.837	0.999	1.018	0.002004	38.64	0.99
-31.818	0.988	0.982	0.001978	37.93	1.19
-29.809	0.965	0.914	0.001951	45.90	1.04
-28.809	0.955	0.880	0.001971	67.71	1.18
-27.790	0.944	0.845	0.002004	67.40	1.17
-26.790	0.934	0.812	0.002034	50.14	1.08
-25.780	0.923	0.779	0.001498	60.55	6.70
-24.780	0.913	0.747	0.002086	52.16	0.75
-23.760	0.904	0.715	0.002111	50.16	0.65
-22.751	0.894	0.684	0.002125	43.88	2.65
-21.751	0.885	0.654	0.002053	44.67	2.06
-20.731	0.876	0.625	0.001999	42.66	3.73
-19.723	0.868	0.598	0.001945	48.22	3.23
-18.703	0.859	0.573	0.001450	47.06	3.07
-17.694	0.851	0.549	0.001875	47.97	0.87
-16.673	0.844	0.528	0.001835	49.62	2.94
-15.666	0.837	0.510	0.001801	57.60	2.89
-14.644	0.830	0.495	0.001800	51.33	0.84
-13.638	0.823	0.483	0.001802	58.21	2.36
-12.615	0.817	0.475	0.001806	59.77	0.51
-11.610	0.812	0.470	0.001858	58.47	1.34
-10.611	0.807	0.470	0.001818	57.34	5.63
-9.584	0.802	0.474	0.001822	68.35	0.43
-8.166	0.796	0.485	0.001812	64.12	3.96
-7.139	0.792	0.498	0.001837	79.84	0.44

-6.140	0.789	0.514	0.001833	64.35	4.07
-5.136	0.786	0.533	0.001873	64.34	3.43
-4.112	0.784	0.555	0.001881	75.77	17.95
-3.112	0.782	0.579	0.001894	49.12	4.74
-2.107	0.781	0.605	0.001899	50.22	0.81
0.922	0.780	0.693	0.001864	53.12	1.05
1.945	0.781	0.725	0.001842	53.05	1.17
2.945	0.782	0.758	0.001829	42.29	1.31
3.951	0.784	0.791	0.001366	53.78	2.27
4.952	0.786	0.824	0.001730	61.19	1.19
5.974	0.788	0.859	0.001682	49.51	1.71
6.974	0.791	0.894	0.001659	77.74	1.29
7.981	0.795	0.928	0.001644	64.07	1.61
8.981	0.799	0.963	0.001641	59.95	1.61
10.002	0.804	0.999	0.001648	67.30	1.32
11.002	0.809	1.033	0.001645	57.05	1.64
27.092	0.937	1.566	0.001444	56.89	4.12
28.092	0.947	1.596	0.001446	58.36	3.13
29.087	0.958	1.626	0.001451	64.98	4.20
30.597	0.974	1.670	0.001457	69.33	2.46
31.764	0.987	1.704	0.001460	64.81	3.45
32.931	1.000	1.737	0.001464	70.42	3.03
34.098	1.014	1.769	0.001468	68.07	3.67

ΔT : Time from perihelion on 23.8 May 2015 UT in days

r : Heliocentric distance (AU)

Δ : Geocentric distance (AU)

g : Solar Lyman- α g-factor (photons s^{-1}) at 1 AU

Q : Daily-Average Water production rates (molecules s^{-1}) from the TRM

δQ : internal 1-sigma uncertainties

Table S8. SOHO/SWAN Observations of C/2014 Q1 (PanSTARRS) and Water Production Rates

ΔT (days)	r (AU)	Δ (AU)	g (s^{-1})	Q (10^{27} molecules s^{-1})	δQ (10^{27} molecules s^{-1})
-46.608	1.189	1.988	0.0018	26.93	3.62
-45.608	1.170	1.966	0.0018	22.96	3.90
-42.608	1.112	1.900	0.0018	30.84	2.94
-40.589	1.072	1.856	0.0018	18.78	4.12
-39.590	1.052	1.835	0.0018	44.69	2.07
-38.589	1.032	1.813	0.0018	36.38	2.23
-37.589	1.012	1.792	0.0018	45.05	1.76
-36.589	0.992	1.771	0.0018	27.24	3.30
-34.589	0.952	1.729	0.0018	20.23	4.36
-12.216	0.477	1.350	0.0018	276.80	1.49
-11.050	0.453	1.337	0.0018	403.70	1.81
-9.883	0.430	1.325	0.0018	514.60	1.31
-7.550	0.388	1.303	0.0017	703.20	1.00
-6.106	0.365	1.290	0.0016	773.80	1.10
-4.939	0.349	1.280	0.0016	1854.00	0.98
-3.773	0.335	1.271	0.0015	2610.00	0.59
13.076	0.495	1.182	0.0017	506.40	0.40
14.286	0.520	1.183	0.0017	224.50	0.52
16.720	0.572	1.189	0.0017	111.90	1.03
17.928	0.598	1.195	0.0017	93.75	1.00
19.139	0.625	1.201	0.0017	98.41	1.10
20.357	0.651	1.209	0.0017	98.86	1.12
21.565	0.677	1.217	0.0017	55.50	1.65
22.773	0.703	1.227	0.0017	45.13	2.21
26.404	0.781	1.262	0.0017	20.72	4.23
27.621	0.807	1.275	0.0017	36.32	3.02
28.829	0.832	1.290	0.0017	30.53	3.17
30.037	0.858	1.305	0.0017	21.56	3.97
31.252	0.883	1.321	0.0017	14.22	6.30
33.668	0.933	1.354	0.0017	22.12	3.77
34.885	0.958	1.372	0.0017	14.72	5.93

ΔT : Time from perihelion on 6.5 Jul 2015 UT in days

r : Heliocentric distance (AU)

Δ : Geocentric distance (AU)

g: Solar Lyman- α g-factor (photons s^{-1}) at 1 AU

Q: Daily-Average Water production rates (molecules s^{-1}) from the TRM

δQ : internal 1-sigma uncertainties

Table S9. SOHO/SWAN Observations of C/2013 X1 (PanSTARRS) and Water Production Rates

ΔT (days)	r (AU)	Δ (AU)	g (s ⁻¹)	Q (10 ²⁷ molecules s ⁻¹)	δQ (10 ²⁷ molecules s ⁻¹)
-127.769	2.235	1.615	0.001525	23.92	8.41
-125.769	2.214	1.634	0.001525	52.89	3.94
-117.781	2.131	1.723	0.001523	78.16	2.92
-116.781	2.120	1.736	0.001523	42.87	4.59
-115.781	2.110	1.748	0.001512	69.42	3.15
-109.796	2.049	1.829	0.001513	71.15	3.69
-108.796	2.039	1.843	0.001513	36.63	6.41
-107.795	2.029	1.857	0.001513	49.30	4.40
-106.795	2.018	1.871	0.001513	67.23	4.43
-105.795	2.008	1.885	0.001513	51.93	4.68
-104.795	1.998	1.899	0.001513	101.40	2.43
-103.795	1.988	1.913	0.001514	93.14	2.97
-102.795	1.978	1.928	0.001514	77.37	3.09
-101.795	1.968	1.942	0.001514	100.60	2.60
-100.795	1.958	1.956	0.001514	74.96	3.48
-99.811	1.948	1.970	0.001514	164.90	1.79
-98.794	1.938	1.984	0.001514	114.40	2.69
-97.811	1.928	1.998	0.001514	109.00	2.50
-96.812	1.919	2.012	0.001515	120.40	2.48
-95.812	1.909	2.026	0.001515	60.18	4.65
-94.812	1.899	2.040	0.001502	131.30	2.38
-93.812	1.889	2.053	0.001502	165.80	2.39
-92.812	1.879	2.067	0.001502	95.00	2.95
-91.812	1.870	2.080	0.001502	109.80	2.68
-90.812	1.860	2.094	0.001503	94.96	3.16
-89.812	1.850	2.107	0.001503	86.47	4.01
-88.812	1.841	2.120	0.001503	107.60	2.74
-87.822	1.831	2.132	0.001503	148.40	2.31
-86.822	1.822	2.145	0.001503	116.40	2.92
-85.822	1.812	2.157	0.001503	97.65	3.26
-84.822	1.803	2.170	0.001504	104.30	3.14
-83.821	1.793	2.182	0.001504	86.85	3.93
-82.821	1.784	2.194	0.001504	133.50	2.68
-81.821	1.775	2.205	0.001504	141.20	2.50
-80.821	1.765	2.216	0.001504	124.10	2.82
-79.094	1.749	2.235	0.001492	147.90	2.61
-78.093	1.740	2.246	0.001492	154.20	2.29

-77.093	1.731	2.257	0.001492	175.10	2.36
-76.093	1.722	2.267	0.001492	180.30	2.12
-75.093	1.713	2.277	0.001492	158.20	2.24
-74.093	1.704	2.286	0.001492	130.30	2.89
-73.093	1.695	2.295	0.001493	150.50	2.40
-72.115	1.687	2.304	0.001493	146.10	2.51
-71.115	1.678	2.313	0.001493	173.30	2.21
-70.115	1.669	2.321	0.001493	130.30	2.88
-69.115	1.660	2.330	0.001482	171.10	2.54
-68.115	1.652	2.337	0.001482	108.10	3.94
-66.092	1.635	2.352	0.001482	156.30	3.18
-65.116	1.626	2.359	0.001482	139.00	2.81
-64.116	1.618	2.365	0.001483	137.80	3.27
-63.116	1.610	2.371	0.001483	196.50	2.14
-62.116	1.602	2.377	0.001483	146.60	3.28
-61.116	1.594	2.382	0.001472	156.70	3.08
-60.116	1.586	2.387	0.001472	129.30	3.50
-59.116	1.578	2.392	0.001472	144.40	2.83
-58.116	1.570	2.396	0.001473	155.50	3.53
-57.116	1.562	2.401	0.001473	248.00	2.64
-56.116	1.554	2.404	0.001473	196.50	4.04
-43.788	1.467	2.417	0.001456	122.80	5.98
-16.734	1.338	2.222	0.001413	326.70	1.94
-15.734	1.335	2.209	0.001414	367.60	1.52
-14.733	1.333	2.196	0.001414	441.10	1.10
-13.733	1.330	2.182	0.001414	356.80	1.40
-12.733	1.328	2.167	0.001410	311.90	1.53
-11.733	1.326	2.152	0.001410	324.00	1.44
-10.733	1.324	2.137	0.001411	283.10	1.35
-9.735	1.322	2.121	0.001407	191.70	1.92
-7.735	1.319	2.089	0.001407	139.50	2.76
-6.735	1.318	2.072	0.001404	104.10	2.95
-5.735	1.317	2.055	0.001404	144.60	2.15
-4.735	1.316	2.037	0.001404	114.80	3.07
-3.735	1.315	2.019	0.001404	148.90	7.10
-1.735	1.315	1.982	0.001403	106.80	3.20
-0.736	1.314	1.962	0.001403	150.10	2.34
0.264	1.314	1.943	0.001403	111.20	2.69
1.264	1.314	1.923	0.001404	144.90	2.07
2.264	1.315	1.903	0.001404	176.10	2.04
3.264	1.315	1.882	0.001404	99.80	2.82
4.264	1.316	1.861	0.001402	102.50	2.94
5.264	1.317	1.840	0.001402	135.70	1.99

6.264	1.318	1.818	0.001403	113.10	2.23
7.249	1.319	1.797	0.001402	108.50	2.43
8.249	1.320	1.775	0.001402	152.50	1.95
9.249	1.322	1.752	0.001402	106.20	2.27
11.249	1.325	1.706	0.001402	131.70	1.81
13.249	1.329	1.660	0.001403	132.20	2.05
14.250	1.332	1.635	0.001402	140.60	1.96
15.544	1.335	1.604	0.001403	117.70	1.45
17.250	1.339	1.562	0.001403	120.30	1.53
18.250	1.342	1.537	0.001404	142.70	2.08
19.250	1.346	1.512	0.001404	134.50	1.67
20.250	1.349	1.487	0.001405	146.20	1.70
21.250	1.352	1.461	0.001406	146.50	1.87
22.250	1.356	1.436	0.001406	141.10	1.89
24.251	1.363	1.384	0.001406	168.60	1.79
30.252	1.390	1.227	0.001413	131.50	1.75
31.252	1.395	1.201	0.001413	127.20	1.53
35.252	1.416	1.096	0.001417	142.30	0.76
40.299	1.445	0.968	0.001424	118.60	14.48
41.299	1.451	0.943	0.001424	109.70	7.33
42.311	1.457	0.919	0.001425	105.20	9.57
46.092	1.482	0.833	0.001432	72.46	2.88
47.083	1.489	0.812	0.001432	54.27	3.41
48.083	1.495	0.791	0.001432	64.64	3.09
49.065	1.502	0.772	0.001439	22.07	7.85
50.065	1.509	0.753	0.001439	67.37	3.93
51.064	1.517	0.736	0.001440	65.49	2.94
52.058	1.524	0.720	0.001440	44.55	3.54
53.058	1.531	0.705	0.001440	40.10	3.95
54.059	1.539	0.691	0.001441	53.03	4.13
55.037	1.546	0.679	0.001449	64.95	3.33
56.037	1.554	0.669	0.001450	47.17	3.35
59.031	1.577	0.648	0.001451	49.53	2.64
60.032	1.585	0.645	0.001451	38.40	4.03
61.032	1.593	0.643	0.001451	28.92	6.40
62.006	1.601	0.644	0.001460	31.03	4.27
63.006	1.609	0.647	0.001461	54.30	2.55
77.247	1.733	0.866	0.001481	30.86	6.35
78.248	1.742	0.891	0.001482	60.45	3.86
101.209	1.962	1.572	0.001504	35.35	7.63
102.222	1.972	1.605	0.001505	27.72	12.55

ΔT : Time from perihelion on 20.8 Apr 2016 UT in days

r : Heliocentric distance (AU)

Δ : Geocentric distance (AU)

g : Solar Lyman- α g-factor (photons s^{-1}) at 1 AU

Q : Daily-Average Water production rates (molecules s^{-1}) from the TRM

δQ : internal 1-sigma uncertainties